

11011

**U. S. A R M Y**  
**TRANSPORTATION RESEARCH COMMAND**  
**FORT EUSTIS, VIRGINIA**

TRECOM TECHNICAL REPORT 64-56

**WIND TUNNEL TESTS  
OF AN OPTIMIZED,  
MATCHED-STIFFNESS RIGID ROTOR**

Project 1D121401A142  
Contract DA 44-177- C-78(T)

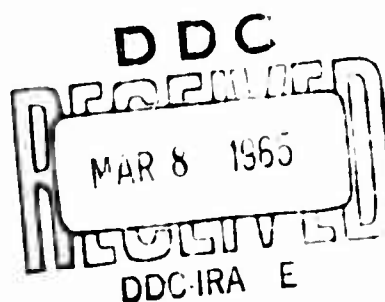
November 1964

COPY	2	OF	3	8740
HARD COPY				\$ 3.00
PHOTOCOPY				\$ 0.75

64-56

**prepared by:**

LOCKHEED-CALIFORNIA COMPANY  
Burbank, California



ARCHIVE COPY

### DISCLAIMER NOTICE

When Government drawings, specifications, or other data are used for any purpose other than in connection with a definitely related Government procurement operation, the United States Government thereby incurs no responsibility nor any obligation whatsoever; and the fact that the Government may have formulated, furnished, or in any way supplied the said drawings, specifications, or other data is not to be regarded by implication or otherwise as in any manner licensing the holder or any other person or corporation, or conveying any rights or permission, to manufacture, use, or sell any patented invention that may be any way be related thereto.

\* \* \*

### DDC AVAILABILITY NOTICE

Qualified requesters may obtain copies of this report from

Defense Documentation Center  
Cameron Station  
Alexandria, Virginia 22314

\* \* \*

This report has been released to the Office of Technical Services, U. S. Department of Commerce, Washington 25, D. C., for sale to the general public.


\* \* \*

The findings and recommendations contained in this report are those of the contractor and do not necessarily reflect the views of the U. S. Army Mobility Command, the U. S. Army Materiel Command, or the Department of the Army.

No DDC limit

HEADQUARTERS  
U S ARMY TRANSPORTATION RESEARCH COMMAND  
FORT EUSTIS, VIRGINIA 23604

This report has been reviewed by this command and is considered to be technically sound. The report is published for the exchange of information and the stimulation of ideas.



JOHN E. YEATES  
Group Leader  
Aeromechanics Group

APPROVED.

FOR THE COMMANDER:



LARRY M. HEWIN  
Technical Director

PROJECT 1D121401A142  
CONTRACT DA 44-177-JMC-78(T)

TRECOM TECHNICAL REPORT 64-56

NOVEMBER 1964

WIND TUNNEL TESTS  
OF AN OPTIMIZED,  
MATCHED-STIFFNESS RIGID ROTOR

LOCKHEED REPORT NO. 17790

PREPARED BY  
LOCKHEED-CALIFORNIA COMPANY  
BURBANK, CALIFORNIA

for

U. S. ARMY TRANSPORTATION RESEARCH COMMAND  
FORT EUSTIS, VIRGINIA

## CONTENTS

	<u>Page</u>
PREFACE	iii
LIST OF ILLUSTRATIONS	vii
TABLE OF SYMBOLS	xi
SUMMARY	1
INTRODUCTION	5
DESCRIPTION OF TEST ARTICLE	7
MODEL	7
ROTOR	7
PHYSICAL PROPERTIES AND SIMULATION	10
INSTRUMENTATION	18
WIND TUNNEL TESTS	19
PROCEDURE	19
RESULTS AND DISCUSSION	21
CONCLUSIONS AND RECOMMENDATIONS	30
DISTRIBUTION	56

## ILLUSTRATIONS

<u>Figure</u>		<u>Page</u>
1	Model in Transonic Dynamics Tunnel, 3-Blade Rotor	2
2	Model in Transonic Dynamics Tunnel, 4-Blade Rotor	3
3	Model in Lockheed Tunnel, 6-Blade Rotor	4
4	Rotor Hub	8
5	Rotor and Control Schematic	9
6	Blade Strain Gage Locations and Typical Sections	11
7	Blade Ballast Installation	12
8	Spanwise Distribution of Blade Properties	14
9	Blade Bending Frequency Spectrum for Air Tests	16
10	Blade Bending Frequency Spectrum for Freon Tests	17
11	Data Point Map	20
12	Model Air/Ground Resonance Frequency Situation	22
13	4-Blade Rotor Loads, 1.5 "g", 0 MPH	31
14	4-Blade Rotor Loads, 1.25 "g", 100 MPH	32
15	4-Blade Rotor Loads, 1.0 "g", 140 MPH	33
16	4-Blade Rotor Loads, .75 "g", 200 MPH	34
17	4-Blade Rotor Loads, 0 "g", 250 MPH	35
18	Twisted Blade Loads, 1.3 "g", 100 MPH	36
19	3-Blade Rotor Loads, .65 "g", 140 MPH	37
20	6-Blade Rotor Loads, 1.25 "g", 150 MPH	38
21	3-, 4-, and 6-Blade Load Comparisons at 140 MPH	39
22	Flexure Hub Rotor Weight Trends	40
23	Forward Speed vs Oscillating Pitch Link Load, 4-Blade Rotor	41
24	Forward Speed vs Oscillating Pitch Link Load, 5-Blade Rotor	41
25	Forward Speed vs Oscillating Pitch Link Load, 6-Blade Rotor	42
26	Forward Speed vs Oscillating Pitch Link Load, 4-Blade (-6° Twist) Rotor	42

# ILLUSTRATIONS (continued)

<u>Figure</u>		<u>Page</u>
27	Forward Speed vs Mid-Flap Cyclic Stress, 4-Blade Rotor	43
28	Forward Speed vs Mid-Flap Cyclic Stress, 3-Blade Rotor	43
29	Forward Speed vs Mid-Flap Cyclic Stress, 6-Blade Rotor	44
30	Forward Speed vs Mid-Flap Cyclic Stress, 4-Blade ( $-6^{\circ}$ Twist) Rotor	44
31	Forward Speed vs Mid-Chord Cyclic Stress, 4-Blade Rotor	45
32	Forward Speed vs Mid-Chord Cyclic Stress, 4-Blade ( $-6^{\circ}$ Twist) Rotor	45
33	Forward Speed vs Inboard-Chord Cyclic Stress, 4-Blade Rotor	46
34	Forward Speed vs Inboard-Chord Cyclic Stress, 3-Blade Rotor	46
35	Forward Speed vs Inboard-Chord Cyclic Stress, 6-Blade Rotor	47
36	Forward Speed vs Inboard-Chord Cyclic Stress, 4-Blade ( $-6^{\circ}$ Twist) Rotor	47
37	Oscillating Mid-Span Flap Stresses vs Forward Speed and Solidity	48
38	Oscillating Pitch Link Loads vs Forward Speed and Solidity	48
39	Oscillating In-Plane Stresses vs Forward Speed and Solidity	49
40	Oscillating In-Plane Stresses vs Forward Speed and Blade Loading	49
41	Vertical Body Vibration vs Forward Speed, 4-Blade ( $6^{\circ}$ Twist) Rotor	50
42	Vertical Body Vibration vs Forward Speed, 4-Blade Rotor	50
43	Vertical Body Vibration vs Forward Speed, 3-Blade Rotor	51

ILLUSTRATIONS (continued)

<u>Figure</u>		<u>Page</u>
44	Vertical Body Vibration vs Forward Speed, 6-Blade Rotor	51
45	Longitudinal Body Vibration vs Forward Speed, 4-Blade (-6° Twist) Rotor	52
46	Longitudinal Body Vibration vs Forward Speed, 4-Blade Rotor	52
47	Longitudinal Body Vibration vs Forward Speed, 3-Blade Rotor	53
48	Longitudinal Body Vibration vs Forward Speed, 6-Blade Rotor	53
49	Lateral Body Vibration vs Forward Speed, 4-Blade (-6° Twist) Rotor	54
50	Lateral Body Vibration vs Forward Speed, 4-Blade Rotor	54
51	Lateral Body Vibration vs Forward Speed, 3-Blade Rotor	55
52	Lateral Body Vibration vs Forward Speed, 6-Blade Rotor	55



### TABLE OF SYMBOLS

R - rotor radius

$\Omega$  - rotor rotational speed

$W_{IC}$  - 1st mode inplane bending frequency

IC - inboard-chord (strain gauge location) - 7.46% R

MC - mid-chord (strain gauge location) - 28.8% R

IF - inboard-flap (strain gauge location) - 4.98% R

MF - mid-flap (strain gauge location) - 33.8% R

I - section moment of inertia - in.<sup>4</sup>

C - distance from neutral axis to extreme fiber - in.

Z - section modulus (I/C) - in.<sup>3</sup>

$\Psi$  - blade azimuth angle, 0° is aft

## SUMMARY

A 10-foot-diameter model of a new type of rigid rotor was tested in the Freon atmosphere of the NASA Langley Transonic Dynamics Tunnel at simulated speeds up to 263 miles per hour.

Configurations having 3, 4, and 6 blades with zero blade twist and a 4-blade configuration with six degrees of negative twist were tested. See Figures 1, 2 and 3. A flexure system eliminated the usual feathering bearings. While a true matched stiffness rotor would have flapping and in-plane stiffness matched along the full length of the blade, the system tested had stiffness matched only in the blade flexure region.

The tests were successful, and this new type of rigid rotor appears to offer substantial advantages over previous stiff in-plane rigid rotors by reducing:

1. Rotor Weight
2. Gyro Weight and Drag
3. Hub Drag
4. Control Forces
5. Mechanical Complexity



FIG. 1 - MODEL IN TRANSONIC DYNAMICS TUNNEL, 3-BLADE ROTOR



FIG. 2 - MODEL IN TRANSONIC DYNAMICS TUNNEL, 4-BLADE ROTOR



FIG. 3 - MODEL IN LOCKHEED TUNNEL, 6-BLADE ROTOR

## INTRODUCTION

This wind tunnel program is a continuation of the rigid rotor research work begun by Lockheed in 1958. More specifically, it is a continuation of the investigation of the matched-stiffness type of rigid rotor reported in May 1964 as TRECOM Technical Report 63-75. In the previous work the matched stiffness rotor was tested and compared to the chord stiff type of rotor design flown on the Lockheed CL 475 test bed and the XH-51 research helicopter. In this comparative type of model rotor testing, a "mechano set" type of rotor was constructed so that a wide variety of rotor parameters could be easily tested. This approach necessarily resulted in a research type of rotor which could not be an optimum from the weight, drag, or simplicity standpoint for any one of the seven configurations tested.

This report describes a follow-on program in which the results of the earlier work were used to design a rotor of the matched stiffness type which was optimized for rotor weight, hub drag, mechanical simplicity and control requirements.

Matched stiffness means that the elastic (but not centrifugal) stiffness of the rotor blades outboard of the point at which feathering occurs is approximately the same chordwise and flapwise. Matched blades are usually designed to have their operating r.p.m. range well above their first or cantilever in-plane natural frequency. This means that the possibility exists of obtaining mechanical instability or "ground" resonance involving any body mode which results in in-plane hub motion and cyclic in-plane blade motion occurring at a frequency equal to the operating rotational frequency minus the first in-plane natural frequency. This phenomenon can occur in flight as well as on the ground with a rigid rotor and is therefore referred to hereafter as air/ground resonance. This phenomenon was studied experimentally as part of this program.

The advantage of blade stiffness matching are:

1. Chordwise blade moments are decoupled from blade feathering. This decoupling eliminates undesirable feedback to the gyro control system. This opens the door to a significant reduction in the size of the control gyro, which in turn means a reduction in control loads, boost requirements, gyro aerodynamic drag and gyro weight.
2. Blade in-plane loads are substantially lower than in a chord stiff design. This was demonstrated in the earlier test work and allows lighter blade designs.

3. The low level of in-plane stiffness required for matching makes this type of rotor suited to the design of a new flexure type of hub in which all bearings are eliminated from the hub. This flexure hub has no bearings, no wear points, no lubrication requirements, and very low drag and weight and is structurally redundant.

One basic blade and hub design was tested in this program. Configurations **having 3,4, and 6 blades were tested with zero blade twist, and a 4-blade** configuration was tested with -6 degrees of blade twist. The only other variations possible were in the control system, where gyro inertia and damping could be varied within limits.

Hovering and low speed (to approximately 35 miles per hour) testing was done in the diffuser section of the Lockheed Power Plant Laboratory Wind Tunnel at Burbank. High speed testing to a simulated 263 miles per hour was done in the Freon atmosphere of the NASA Langley Research Center Transonic Dynamics Wind Tunnel.

## DESCRIPTION OF THE TEST ARTICLE

### MODEL

The wind tunnel model constructed for the previous program and described in TRECOM Technical Report 63-75 was used with the following modifications.

The rotor control system was completely redesigned to install the very small gyro that was now feasible inside the body shell. Use of the small gyro was dependent on obtaining low friction levels in the control system. To accomplish this, all plain type bearings were eliminated in the rotating control system and in the gyro gimbal through the use of instrument ball bearings and flexures elements. Gyro to blade pitch links were made C shaped, as shown in Figure 4, to lie close to the rotor shaft and to present minimum frontal area for drag. The gyro consisted of nothing more than the rotating portion of the minimum sized swashplate. Two silicon fluid filled viscous dampers were provided 90 degrees apart in the nonrotating control system.

Pitch and roll trim forces were applied to the swashplate by two 4-inch-diameter bellows assemblies placed 90 degrees apart in the nonrotating system. Air pressure in the bellows could be varied above and below ambient by the model controller to obtain positive and negative moments on the swashplate. A quick change arrangement allowed the trim power available to be changed by a factor of 5.5 through the use of either the 4-inch bellows or a smaller bellows. The 4-inch bellows were used throughout the tests described in this report. These bellows produced a spring rate on the swashplate of approximately 3.2 inch-pounds per degree of angular motion of the swashplate with respect to the shaft.

The body shell was made 2 inches deeper to accommodate the swashplate on top of the rotor shaft bearing box. Fairings shown in Figures 1 and 2 were installed on the hub and around the rotor shaft to minimize drag and rotor/body interference effects.

During the Burbank hovering and low-speed test phase a Denison hydraulic motor replaced the three synchronous electric motors which powered the rotor in the high-speed test phase.

### ROTOR

The 10-foot-diameter, matched-stiffness, flexure hub rotors tested in this program consist of 3-, 4-, or 6-blade/flexure assemblies which are bolted between a pair of flanges on the rotor shaft. See Figure 5. The outer 70 percent of the blade span consists of a laminated, stainless-steel, bonded D-spar which constituted the leading 30 percent of the 3.75-inch chord. The trailing edge is constructed of contoured aluminum honeycomb with .003" aluminum skins. The trailing edge is slotted every 3 inches, and the slots are filled with a flexible polyurethane foam to prevent aerodynamic leakage and to provide in-plane damping of second and higher mode blade motion.



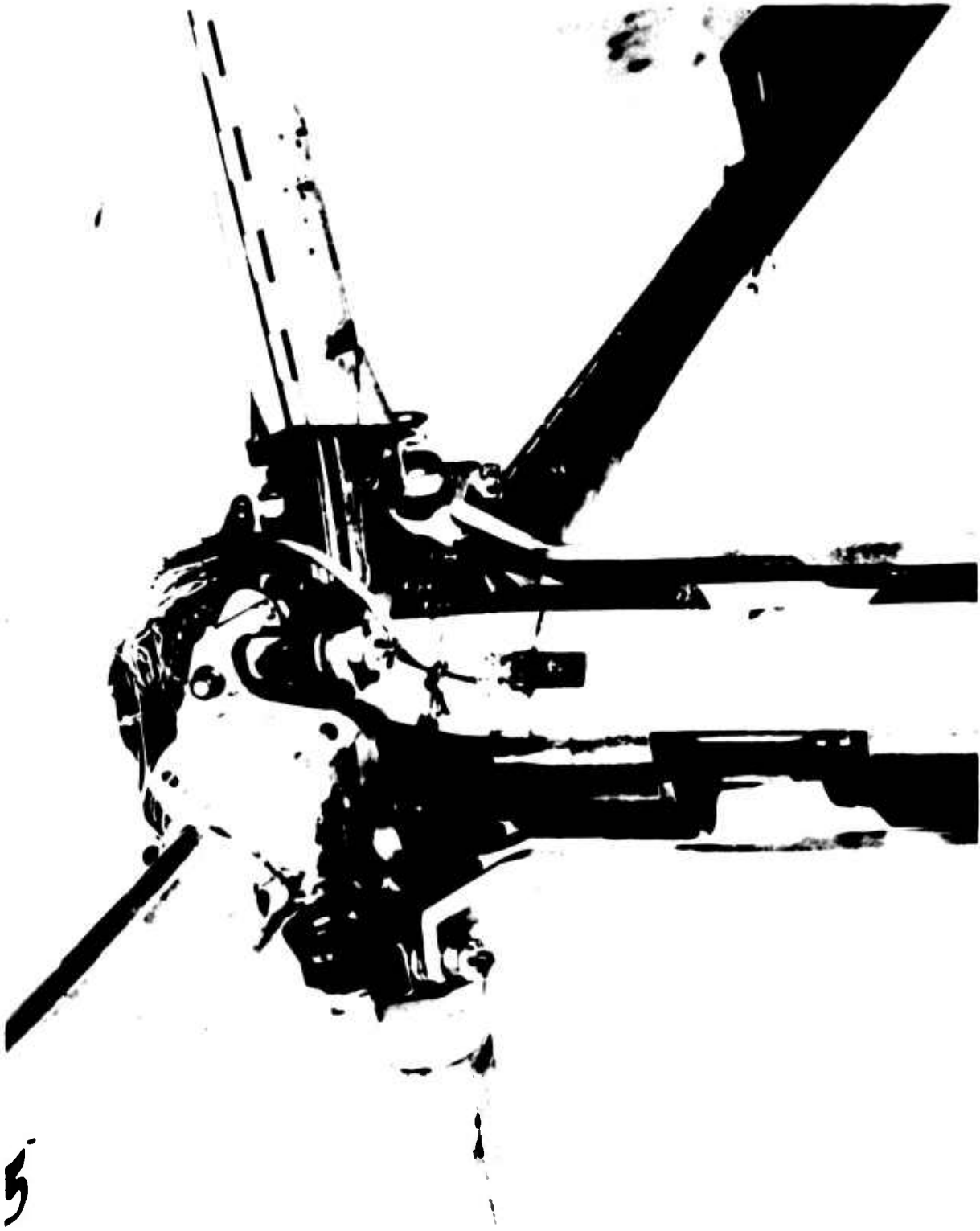


FIG. 4 - ROTOR HUB

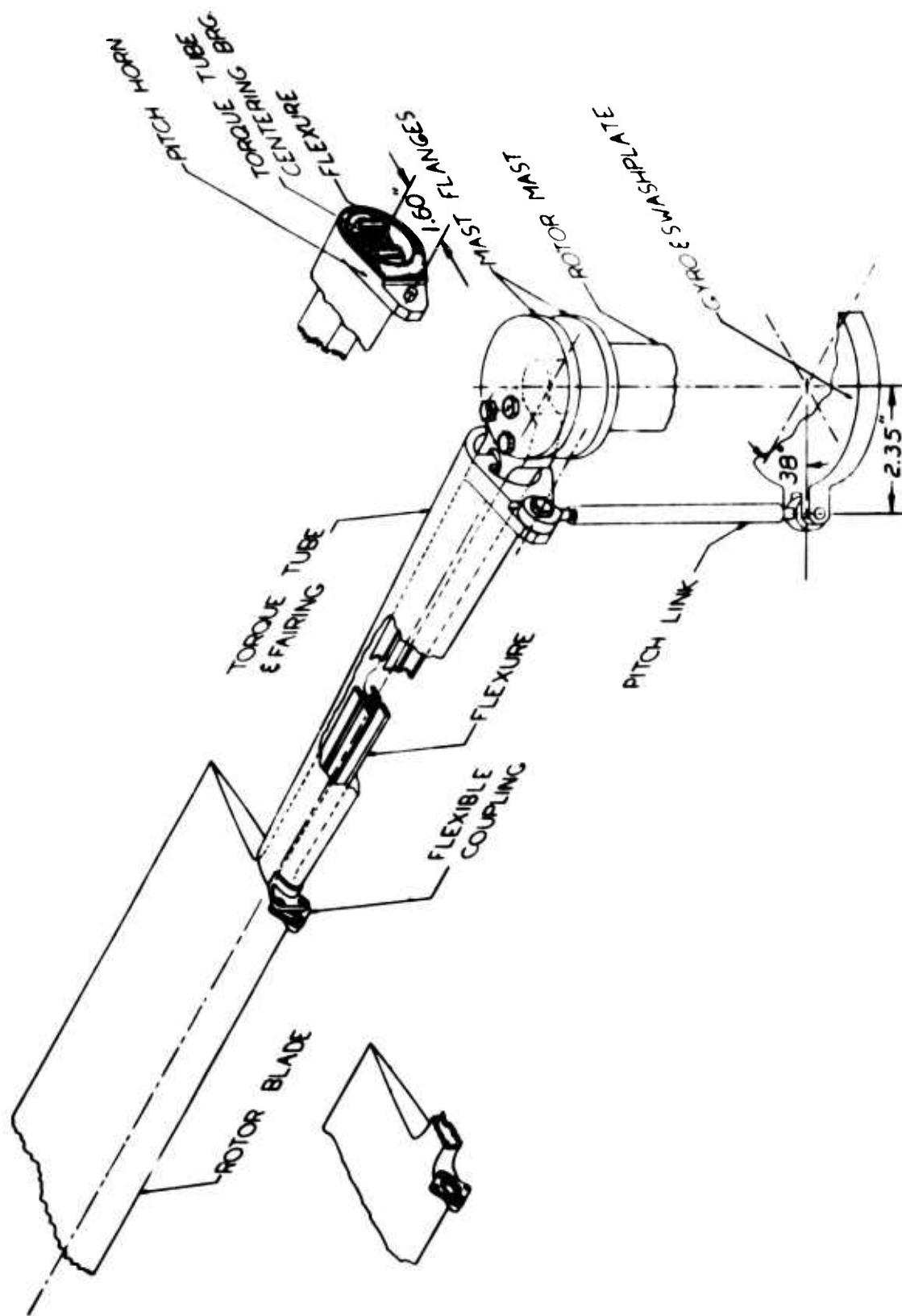


FIG. 5 - ROTOR AND CONTROL SCHEMATIC

The inboard 30 percent of the blade span is the flexure. The flexure is a laminated, bonded, stainless-steel, modified X-section which evolves from the D-spar and completes an integral, jointless, structurally continuous member from blade tip to shaft attachment. The flexure has essentially the same stiffness in-plane as flapwise and is torsionally soft enough to accommodate  $\pm 15$  degree changes in blade feathering angle. Machined fittings are bonded to the inboard end of the flexure to accommodate the three bolt attachment to the rotor shaft. Typical blade and flexure cross sections are shown in Figure 6.

A combination aerodynamic fairing and control torque tube covers the flexure and attaches to the D-spar at 30-percent span with a small Thomas type flexible coupling. This coupling is rigid with respect to blade feathering torsion but will not transmit any appreciable in-plane or flapwise bending moments into the torque tube. The inboard end of the torque tube has a laminated steel flexure plate which accommodates in-plane and flapping motions of the blade and which contains two ball bearings. One ball bearing attaches to the pitch link and the other is anchored to the hub. Between them they convert pitch link forces into feathering torsions and vice versa.

The blade section was a constant 3.75-inch-chord NASA 631A012 (130 mean line) section with either 0-degree twist or -6 degree linear twist nose-down from shaft to tip. No twist was present in either the flexure or the torque tube, so the twist was actually -4.2 degrees from 30 to 100 percent radius.

The blades were converted from the air test to the Freon test configuration by the addition of ballast assemblies and plastic fillers added into the D-spar and X-section as shown in Figure 7.

## PHYSICAL PROPERTIES AND SIMULATION

The physical properties of the model and rotor are given in Table 1 and Figure 8. This type of generalized model testing can be scaled to any size that is of interest. However, the particular simulated full-scale vehicle that was used as a scaling and design reference in order to insure that the model design represented a realistic configuration is shown with the applicable scale factors in Table 1. The model in Freon matches the full-scale simulated vehicle exactly in Mach number, Reynolds number and dynamic pressure ( $q$ ). Further, the Strouhal number is matched, which means that the reduced frequency is matched and therefore the full-scale dynamic effects are represented. Froude number, however, is not matched. This parameter may be interpreted in this case as a ratio of vehicle kinetic energy to gravitational potential energy. Therefore, model height loss to speed gained is not scaled to the full-scale vehicle. This has an effect on the low-frequency stability of a vehicle in free flight. However, the spring rate and limited travel of the model on the

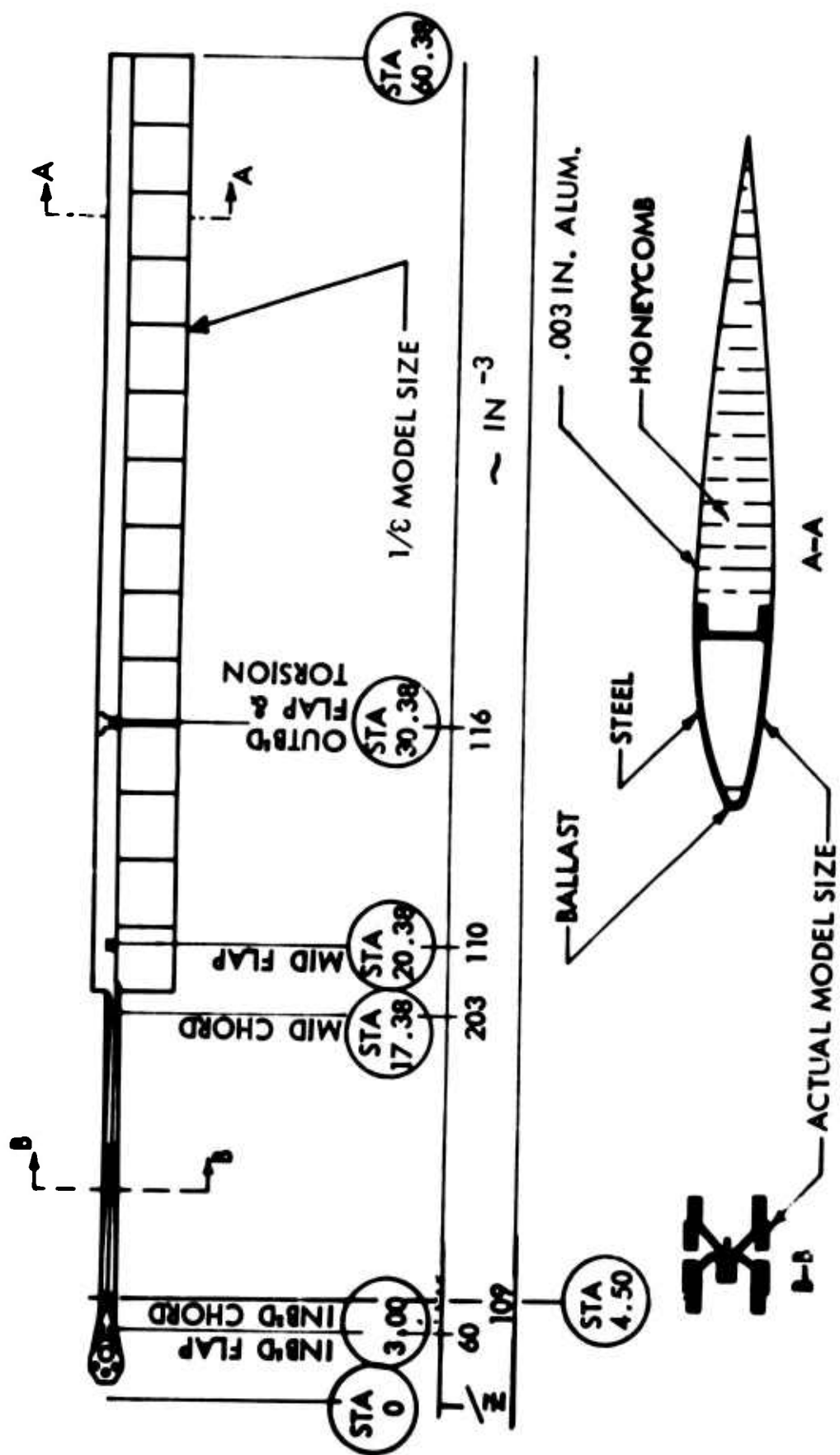
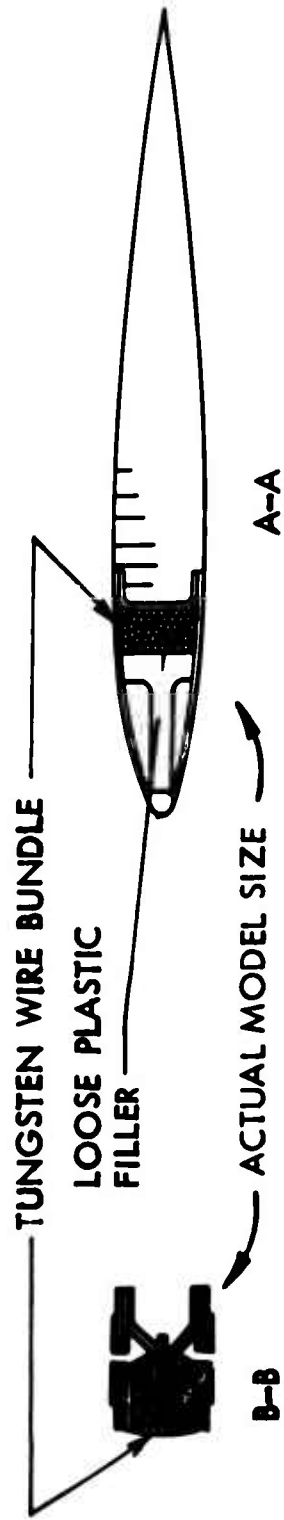
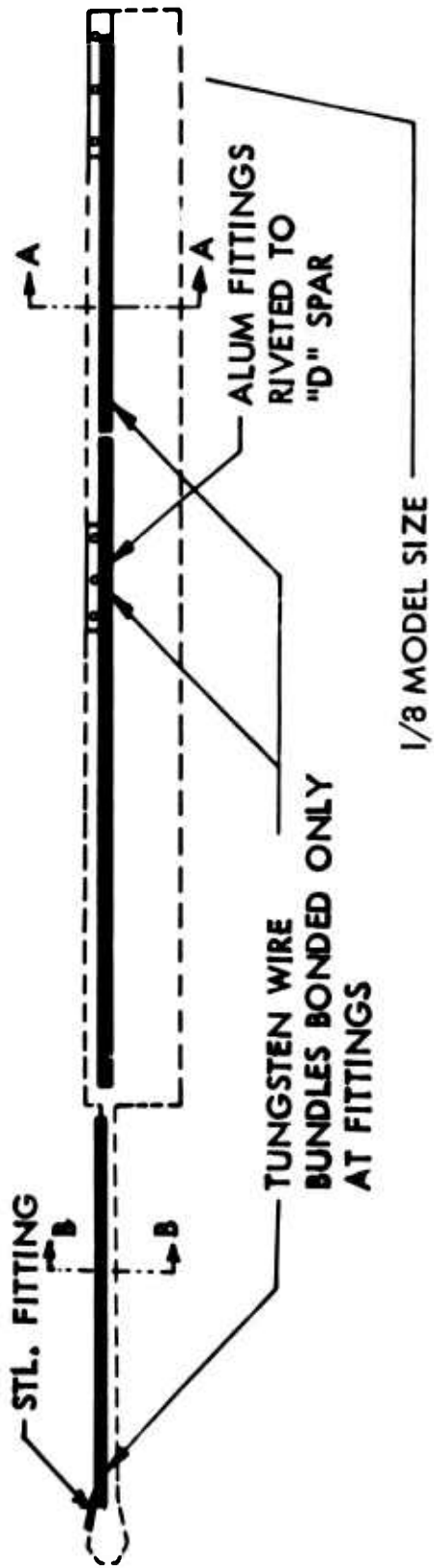


FIG. 6 - BLADE STRAIN GAGE LOCATIONS & TYPICAL SECTIONS



**FIG. 7 - BLADE BALLAST INSTALLATION**

TABLE 1 PHYSICAL PROPERTIES AND SIMULATION

	Model In Air	Scale Factor	Model In Freon	Scale Factor	Simulated Vehicle
Number of Blades	4	1	4	1	4
Blade Chord	.312'	1	.312'		.855'
Rotor Diameter	10'	1	10'	2.75	27.5'
Rotor Area	78.5	1	$78.5 \left(\frac{D_V}{D_M}\right)^2$	7.55	595
Solidity	.08	1	.08	1	.08
Pitch Inertia	$6.30 \left\{ \frac{\rho_{Freon}}{\rho_{Air}} \right\}$		$21.9 \left\{ \frac{\rho_{Air}}{\rho_{Freon}} \times \left(\frac{D_V}{D_M}\right)^5 \right\}$	36.7	805
Roll Inertia	$1.14 \left\{ \frac{\rho_{Freon}}{\rho_{Air}} \right\}$	3.47	$3.90 \left\{ \frac{\rho_{Air}}{\rho_{Freon}} \times \left(\frac{D_V}{D_M}\right)^3 \right\}$		
Mass	142		$494 \left\{ \frac{\rho_A}{\rho_F} \times \left(\frac{D_V}{D_M}\right)^3 \right\}$	4.85	2400
Rotor Lift	$388 \left\{ \frac{q_{Freon}}{q_{Air}} \right\}$	.82	$318 \left(\frac{D_V}{D_M}\right)^2$	7.55	2400
Disc Loading, psf	4.95		4.04	1	4.04
Tip Speed & rpm	650 & 1242		315 & 603		650 & 1242
Altitude & Temp.	1000' Std.		1100'		8000' Std.
Speed of Sound, fps	1113		525		1154
Density	.00230		.0080		.00187
Blade $R_N \odot V_t$	1,250,000		2,920,000	1	2,920,000
" $q \odot V_t$ , psf	485		396	1	396
Mach No. $\odot V_t$	.585	1	.60	1	.60

\*Desired value for correct simulation

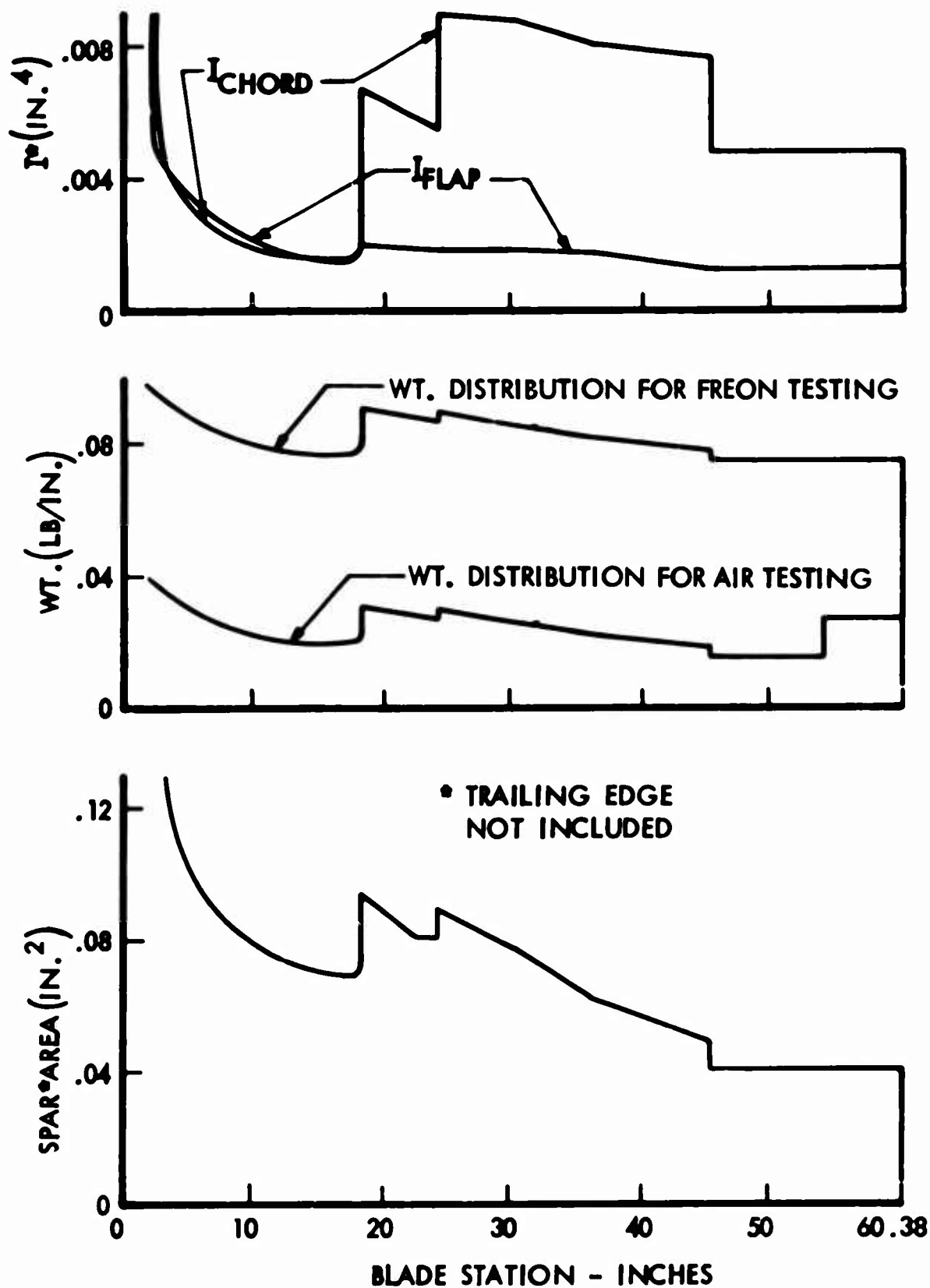


FIG. 8 - SPANWISE DISTRIBUTION OF BLADE PROPERTIES

support system impose added restrictions on the investigation of this area; therefore, model results in this particular area are of limited use.

Table 1 relates the model 4-blade configuration to a simulated vehicle with a 4-blade rotor. The 3-blade and 5-blade configurations represent the application of higher and lower blade numbers and solidity to this same simulated vehicle.

In order to simulate the largest possible vehicle with the model in Freon, it was desirable to use the highest possible tip speed with the highest available Freon density to obtain maximum Reynolds number. A hovering tip Mach number of 0.60 was selected as representative of current rotor design practice, as this can be interpreted as a 700 fps tip speed at 105 degrees F. or a 650 fps tip speed at 28 degrees F. This tip Mach number used with the highest available speed of sound in Freon determined the rotor tip speed (and the velocity scaling) in Freon. This speed scaling determined the maximum dynamic pressure available.

A design tip speed of 650 fps was selected for the model in air and the simulated vehicle as being representative of current rotor design practice.

In testing the model in air at this tip speed, the tip Mach number is slightly low but the dynamic pressure is high. For proper scaling, all angles must stay constant. Using the same blade angles as in Freon (and as on the simulated vehicle at 8,000-foot standard day) and the higher dynamic pressure available in the air tests will result in increased rotor lift and thus higher disc loading to simulate the same dynamic situation. The coning angle will scale correctly if the blade mass to fluid density ratio is held constant, because

$$\text{coning} = \frac{\text{Lift}}{\text{Centrifugal Force}} = \frac{\text{Fluid Density} \times \Omega^2}{\text{Blade Mass} \times \Omega^2}$$

This meant that in taking the model from air at  $\rho = .0023$  into Freon at  $\rho = .0080$ , the blade mass had to be increased by a factor of 3.47.

The blade natural frequency to design r.p.m. ratios from the model in air are exactly the same as for the simulated vehicle. The air test frequency map is shown in Figure 9. Unfortunately it did not prove possible to increase the blade mass by a factor of 3.47 without also slightly increasing the blade stiffnesses. This resulted in the raising of second and third mode frequencies in the Freon test configurations. The Freon test frequency map is shown in Figure 10. As the blades tested have almost no structural damping of flapping modes or first (cantilever) in-plane mode, it was possible to verify most of the intersection points on the frequency maps by taking continuous oscillograph records while the rotor was run through the r.p.m. range.



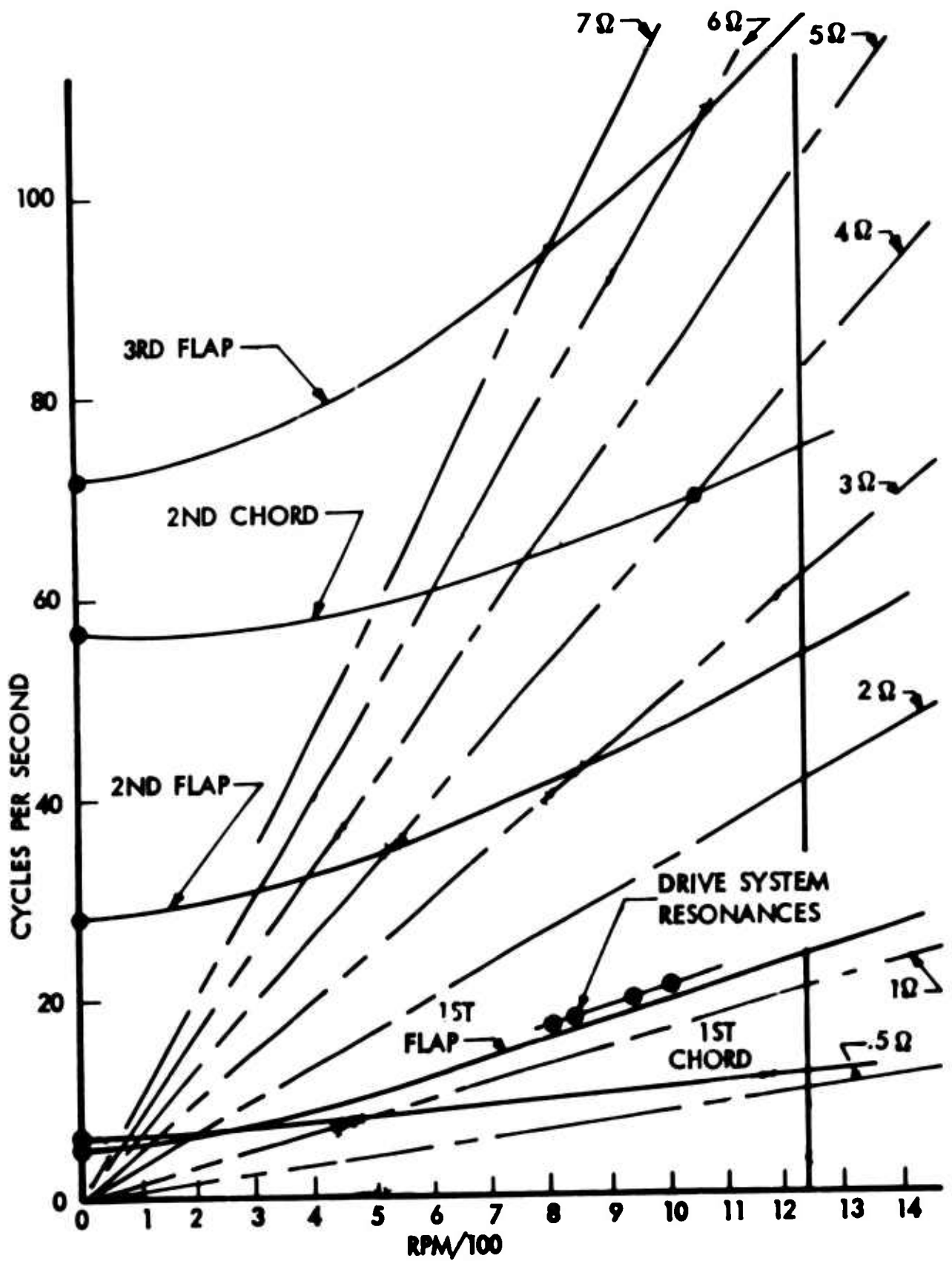


FIG.9 - BLADE BENDING FREQUENCY SPECTRUM FOR AIR TESTS

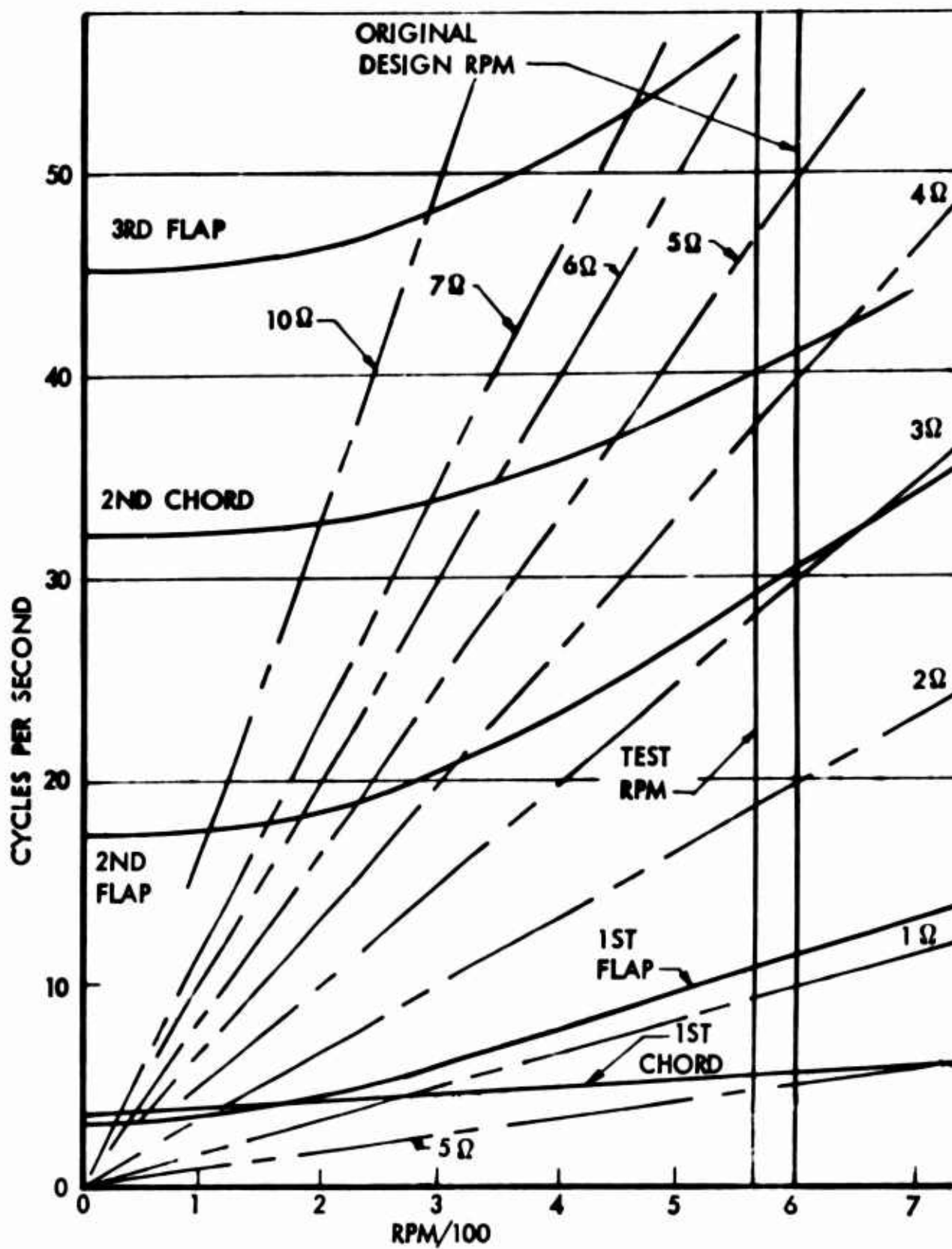


FIG. 10 - BLADE BENDING FREQUENCY SPECTRUM FOR FREON TESTS

Because of the necessity of restraining the body motions of the wind-tunnel model through a spring suspension system, the mass and inertia scaling of the model body is not particularly meaningful. The springs have the effect of raising the body mode natural frequencies and changing the response of the body to forcing functions from the rotor.

Forces measured on the model either in air or in Freon can be scaled to other vehicle sizes simply by multiplying by the square of the scale factor. For example, a pitch link load of 10 pounds on the model would be

$$10 \text{ lb.} \times \left( \frac{35 \text{ ft.}}{10 \text{ ft.}} \right)^2 = 122.5 \text{ lb. for a vehicle with a 35-foot diameter}$$

rotor in the same flight condition. Because material areas also scale with the square of the scale factor, stresses shown in this report are independent of scale factor and should remain the same for any size of vehicle which operates at the same tip speeds used in these tests.

### INSTRUMENTATION

The instrumentation both for data recording and for model condition display to the model operator was essentially identical to that used in the previous program and described in TRECOM Technical Report 63-75. A strain-gage measurement of rotor shaft torsion was added.

Figure 6 shows the locations of the blade load measurements, which were all strain gage measurements except blade feathering angle position, which was from a strain gaged cantilever leaf spring follower.

Two strain gaged blades were included in each rotor tested. Data from one blade was fed to the oscillograph while that from the other blade was tape recorded for harmonic analysis by NASA personnel.

## WIND TUNNEL TESTS

Hovering and low-speed (to approximately 35 miles per hour) testing was conducted in February 1964 in the diffuser section of the Lockheed Power Plant Laboratory Wind Tunnel, as shown in Figure 3. The tunnel is approximately 19 feet square at the point where the model was mounted. The rotor plane was 8 feet above the floore. Air-flow velocity through this portion of the tunnel tended to fluctuate such that at a mean velocity of 35 miles per hour the flow-velocity-measuring Pitot reading was varying  $\pm 5$  miles per hour. This caused the model to oscillate in pitch and roll. Pitching velocities as high as 5 degrees per second were recorded. While this rough air was an excellent checkout of the functioning and blade stability of the model, the data collected must be considered as more representative of helicopter flight in rough air than of steady-state smooth flight conditions.

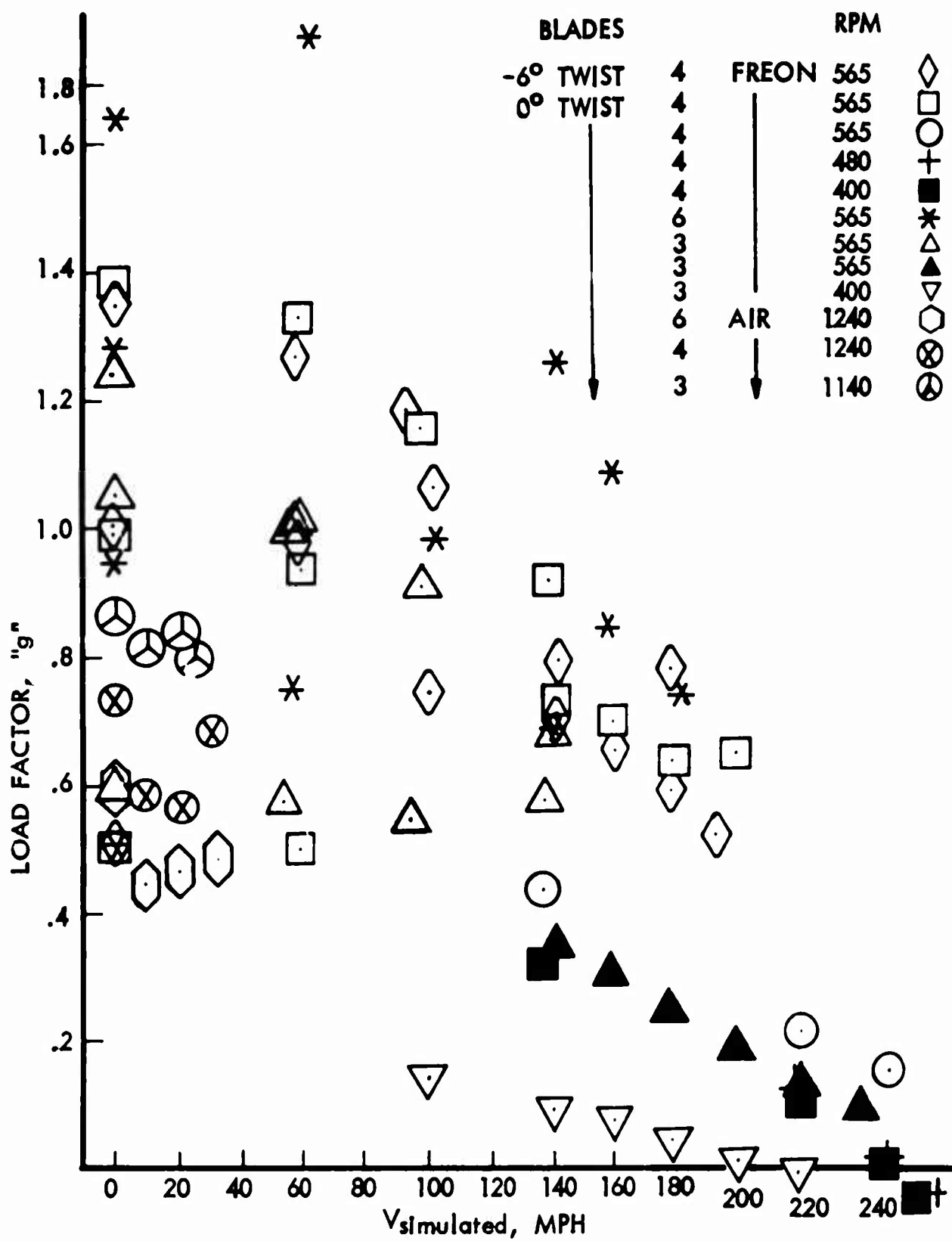
In March 1964, wind-tunnel tests at simulated speeds up to 263 miles per hour were conducted in the Freon atmosphere of the NASA Langley Research Center Transonic Dynamics Wind Tunnel. Helicopter and unloaded rotor flight regimes were tested for 3-, 4-, and 6-blade configurations with zero blade twist and a 4-blade configuration with -6 degrees of blade twist. The 3- and 4-blade configurations are shown in Figures 1 and 2.

Figure 11 shows the distribution with speed and load factor of the 84 data points used in this report.

### PROCEDURE

The general testing procedure was to bring the rotor up to the desired r.p.m., increase collective pitch to obtain the desired hovering lift, trim out any moments on the rotor with the trim system, and record hovering data. The tunnel was then started and brought up to the desired speed. Model pitching attitude and collective pitch were adjusted to obtain the desired flight condition, rotor moments were trimmed out, and data was recorded. At preselected flight conditions the model attitude was then changed nose up and/or nose down, and data was recorded to study the pitching stability of the model. Some of these attitude changes were "untrimmed", in that rotor moments were allowed to build up within safe limits as the model attitude was varied, and the data as recorded contains these moments. Other "trimmed" attitude change data was taken with the rotor moments trimmed out after the attitude change had been made.

At high tunnel speeds it was not feasible to change collective pitch because of a pitch-up phenomenon described later in this report. Most of the data collected at 140 miles per hour (simulated) and above was taken by setting the collective, increasing the tunnel speed, and changing model pitching attitude to vary rotor lift.



## RESULTS AND DISCUSSION

### Air/Ground Resonance

In both the air and Freon test configurations, it was possible by adjustment of the body pitch and roll frequencies to obtain and then to eliminate the ground resonance phenomenon. A typical resonance map is shown in Figure 12. Resonance occurred when a body natural frequency such as roll or pitch, which allows hub in-plane motion, crossed the  $\Omega - w_{ic}$  line. In spite of the fact that blade in-plane damping was extremely low and an effort was made to minimize body pitch and roll damping, it was not possible to detect resonance which should have occurred below 90 percent of design r.p.m. A case in point is the body pitch crossing shown in Figure 12, which should have created a resonance around 400 to 500 r.p.m.

In probing for air/ground resonance, the r.p.m. was slowly increased. As the rotor approached a resonance, a gradual build-up in the amplitude of the in-plane blade loads would occur first, followed by a build-up in body motions. It appeared that the blade first had to "lock on" to the  $\Omega - w_{ic}$  frequency before it could begin to feed energy in the resonant body mode. In one case a drive system resonance where all the blades were oscillating in plane at about 1.27 P apparently hindered the blade's "locking on" to the  $\Omega - w_{ic}$  frequency. Two consecutive oscillograph records were taken with no measurable difference in rotor r.p.m. The first record shows the 1.27 P in-plane drive system resonance and no sign whatsoever of air/ground resonance. The second record taken a few seconds later shows a classic ground resonance situation. It is conjectured that ground resonance is more likely to occur in a hovering situation, where 1 P in-plane excitation is not present, than in forward flight, where the blade must overcome the 1 P excitation in order to "lock on" to the lower  $\Omega - w_{ic}$  frequency. It appears that very little separation of frequencies is necessary to preclude air/ground resonance. The bulk of the Freon tunnel testing was done at 565 r.p.m., where from Figure 12 it appears that  $\Omega - w_{ic}$  was about 3.7 cps and body roll was about 4.9 cps.

### Gyro Control System Operation

At simulated speeds up to 140 miles per hour, the automatic cyclic pitch trimming characteristics of the gyro control system functioned perfectly. It was possible to change tunnel simulated speed from 90 to 140 miles per hour without touching the model trim controls. At 140 miles per hour, the model pitching attitude could be varied from 3 degrees nose down to 2 degrees nose up, again without touching the trim controls or generating any significant rotor moments.

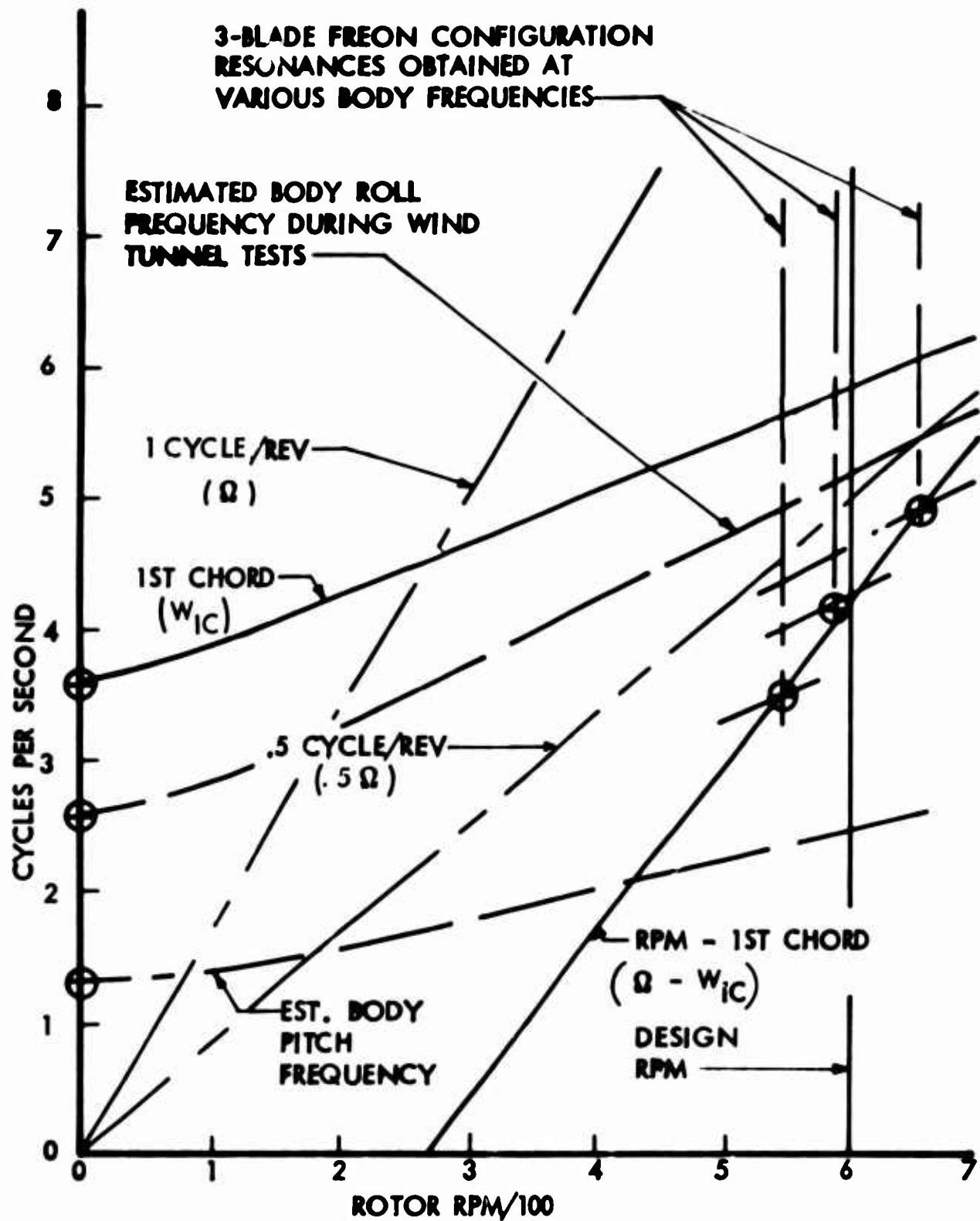


FIG. 12 - MODEL AIR/GROUND RESONANCE FREQUENCY SITUATION



The gyro inertia value used throughout the test program was the minimum value that could be physically obtained, as it was simply the inertia of the minimum-size swashplate and pitch links that were practical to build for the model. Taking the gyro inertia per blade and scaling up to the size of an XH-51 for comparison, the gyro tested was 1/40 the size of that currently flown on the XH-51. There was no indication in any of the tests that this was a marginal size or that it represented the minimum practical gyro size.

Moments applied to the gyro to trim out undesired rotor moments in pitch and roll were extremely small. Except at the highest tunnel speeds, a positive reaction of model pitch or roll moment readout could be obtained for a moment input to the gyro of approximately 1/8 inch-pound.

There was no significant gyro wobble or indication that the gyro caused or participated in the blade "out-of-track" or pitch up incident described later in this report.

The oscillating portion of the pitch link loads was very small in spite of the fact that no negative springs were used to cancel out the blade flexure torsional elastic stiffness of 0.4 inch pound/degree per blade.

Pitch link loads are plotted versus forward speed from the four rotor configurations in Figures 23 through 26. Trend lines with load factor are developed and summarized for 1.0 "g" lift in Figure 38. It is of interest that the pitch link loads for the twisted blade rotor did not rise as rapidly with speed as for the untwisted rotor. The 6-blade-rotor link loads seem to be lower than could be explained on the basis of lower blade loading alone.

Blade torsion load measurements at 50 percent of blade radius are shown by trace number 14 in Figures 13 through 20 to be similar to the pitch link load. In magnitude they are insignificant.

### Pitch-Up

The pitching instability of the model that had been encountered in the previous program was again a problem. Since this is a wind-tunnel model problem and not a flight vehicle problem, it was decided to stabilize the model in pitch with the model mounting springs rather than to build more stability into the rotor than would be required in the rotor of the simulated full-scale vehicle. The model mounting springs were adequate for all attitudes at the lower speeds, but were inadequate for nose-up pitch attitudes at high speeds because of a nonlinear aerodynamic moment variation with model attitude.



Several times in the course of the program, at higher speeds and load factors, the stability boundaries were exceeded inadvertently and the model got away from the operator and pitched up against the stops. Under this condition there is a high probability of breaking blades, as the rigid rotor has the capability of producing more moment than it is designed to withstand. Here, again, the solid pitch and roll stop restraints on a wind-tunnel model represent a situation that does not exist for a free flight vehicle.

A typical case occurred with the 6-blade configuration at one "g" lift and 180 miles per hour. The model pitched up against the stops, and recovery was effected by running the model attitude nose-down. The rotor was retrimmed, oscillograph records were taken and examined for signs of blade damage, and it was concluded that no damage had occurred. Tests continued up to 200 miles per hour. After the rotor was stopped and the tunnel pumped out, it was found that all six blades had been broken in an upward bending sense. The breaks were of the "green twig" variety where bending strength was lost but sufficient material remained in the highly redundant flexure to carry the centrifugal forces. The surprising part of these incidents was that the rotor still responded to trim control and was "flyable" after the blades were "broken" in a flap bending sense.

#### Forward Speed Limitations

Blade stresses were monitored during the tests, and testing was terminated when stresses beyond the endurance limit were encountered. This was usually due to combinations of advance ratio and load factor that resulted in appreciable blade stall and was usually accompanied by an increase in blade tip "out of track".

In the case of the unloaded rotor tests, however, a spurious forward speed limitation occurred. In the near-zero-degree pitching attitude used for the unloaded rotor tests, the model body had no tendency to pitch up or down as speed was increased up to 200 miles per hour simulated. Above this speed the tare measurements (with blades removed) indicated a tendency of the body to pitch nose-up, which was probably even worse with the blades on. The model operators console readout of pitching moment by which he "trimmed" the model was the total of all the moments on the model. Subsequent study of the oscillograph records showed that the model was being held in pitch trim by large nose-down moments supplied by the rotor apparently to overcome the body pitch-up tendency. The high blade stresses that limited forward-speed testing to about 260 miles per hour simulated were 1 P flapping stresses as shown in trace numbers 12 and 13 of Figure 17. This is typical of all the unloaded rotor records above 200 miles per hour. Had a trim capability been incorporated in the horizontal tail to trim out these body moments, it is almost certain that much higher unloaded rotor forward speeds

could have been attained. At the highest tunnel speed reached, the rotor was carrying over 1000 inch-pounds of moment. This is two and one-half times the design steady moment and would correspond to an 11 inch aft c.g. condition on an XH-51. It is not surprising that the model vibration levels were high under these conditions.

Because of these large rotor moments which should not have been present, no attempt is made to draw conclusions regarding the loads and stresses for the unloaded rotor data included in Figures 23, 24, 27, 28, 31, 33, and 34.

### Blade Loads and Stresses

Typical oscillograph traces are shown in Figures 13 through 21. The locations of the strain gages on the blade and the corresponding  $1/z$  values are shown in Figure 6. The stress at the strain-gage location as plotted in Figures 23 through 40 is simply the  $1/z$  value times the bending moment measured by the strain gages.

The rotor blade was designed to be as light as appeared feasible. No "beef" was added to reduce the stresses at high speeds, as one of the purposes of the program was to explore the relationships of solidity, number of blades, and blade loading with forward speed.

Stresses in the blade flexure area could be reduced by adding material to increase the Z value ( $\frac{I}{C}$ ) while holding the section I value constant. However, a 30-percent reduction in stress levels would result in approximately a 30-percent increase in flexure weight.

The cyclic inboard flap bending measurements are not directly comparable between rotor configurations, as their principal content is the 1 P flap bending due to any slight untrimmed rotor moment. As it was not feasible to trim the rotor moment exactly to zero for each data point, any attempt to compare the secondary effects of number of blades, etc., would be very questionable. However, since the 1 P flap bending due to rotor moments dies out approximately as the 4th power of the radius, meaningful comparisons of flap bending at the mid flap gages located one third of the way out from the hub are possible.

In Figures 27 through 30, the mid-flap cyclic stresses are plotted and stress trend lines with load factor and forward speed are developed. Figure 37 compares these stresses at 1 "g" load factor for the four rotor configurations. These stresses are quite low and did not appear to be affected by blade twist. Reduction in blade loading reduced the stresses slightly at low speeds and considerably at higher speeds. The

inboard chord stresses are treated similarly in Figures 33 through 36 and 39. The twisted blades show higher stresses up to about 30 miles per hour, but above this speed the twisted blades show lower stresses than the untwisted blades. At a stress level of about  $\pm 12,000$  psi, it appears that the twisted blades have a 30-miles-per-hour advantage over the untwisted blades. Figure 40 compares these stresses on the basis of common blade loading.

Mid-chord stresses were obtained only for the 4-blade-rotor straight-blade configurations and are shown in Figures 31 and 32. The mid-chord stress trend curves of Figure 31 bear a close family resemblance to the inboard-chord stress curves of Figure 33, as do the mid-and inboard-chord stress curves of the twisted blades in Figures 32 and 36. The twisted blades again show definitely higher forward speeds for the same stress levels as the untwisted blades. This speed increment due to twist is 40 miles per hour at a  $\pm 10$ -ksi stress level and 1 "g" and 65 miles per hour at 0.75 "g".

#### "Blade Out-of-Track" at High Forward Speeds

One of the principal operational problems of testing rotors in a Freon atmosphere is blade tracking. The rotor as ballasted for Freon but operated in air can be operated only in the lower r.p.m. range associated with testing in Freon. The dynamic pressures are so low that the aerodynamic forces generated by the blades are not sufficient to indicate accurately the small difference between blades which cause "out-of-track". Thus, it was necessary to fill the tunnel test section with Freon in order to obtain a meaningful tracking run and to pump out the Freon in order to enter the section to make a track adjustment. This process consumed three to five hours per adjustment. Because of the pressure of time in the tunnel and the desire to test a number of rotor configurations, it was not feasible to take the time that would have been required to obtain perfect blade tracking. Slight "out-of-track" in hovering means that the blades are not carrying exactly the same lift. This slight difference in loading in conjunction with slight differences in blade shape, roughness and effective camber leads to blade-tracking changes with forward speed which usually get much worse at high advance ratios. This was true with the model. For high-speed flight of a full-scale vehicle, it is usually necessary to provide small fixed tabs along the trailing edge of the blades so that small aerodynamic differences between blades can be corrected.

#### Body Vibration

Vibration levels for vertical, longitudinal, and lateral body motions are depicted graphically in Figures 41 through 52. These levels are plotted in the form of amplitude (expressed in  $\pm$  "g") versus forward speed (expressed in miles per hour). The amplitude values presented are those for the simulated vehicle and are obtained by scaling the model data in the following manner.

$$A_{\text{sim veh}} = A_{\text{model}} \frac{\left(\frac{\text{Force}}{\text{Mass}}\right)_{\text{sim veh}}}{\left(\frac{\text{Force}}{\text{Mass}}\right)_{\text{model}}} = 1.56 A_{\text{model}}$$

The model data was obtained from a harmonic analysis performed by NASA of the body accelerometer records. The amplitudes plotted are one half the sum of the amplitudes of the first nine harmonic terms. One case was plotted, and the difference between the amplitude, as expressed by the method used, and the actual curve amplitude with exact phasing is about two percent. The square root of the sum of the squares also gives approximately the same value.

The 6-blade rotor configuration produced the least body vibration. With respect to vertical and longitudinal body vibration levels, the 6-blade rotor was followed by (in order of increased vibration) the 4-blade (-6° twist), 4-blade, and 3-blade rotors. With respect to lateral vibration the 6-blade rotor was followed by the 3-blade, 4-blade (-6° twist), and 4-blade rotor.

Table 2 shows the relative contribution of the different harmonics for the rotor configurations tested. The 1/rev harmonic content of the vibration is largely the product of:

1. Rotor unbalance
2. Rotor blades out of track
3. Rotor produced moments

These factors were present in small but varying amounts for all configurations and test points. The 1/rev content of the vibration should be ignored in comparing configuration, as the above factors do not relate to rotor configuration as such. Both 4-blade rotor configurations show a 4/rev vertical vibration. This may have actually been a pitching and/or rolling acceleration due to the fact that it was physically impossible to place the vertical accelerometer on a vertical line thru the center of gravity. If it was indeed a pitch and/or roll two possible sources exist.

- (1) Blade passage aerodynamic load on the aft part of the body shell.
- (2) The 3/rev, 2nd flapping mode near resonance in the rotating system which can become a cyclic mode (producing moments but not vertical forces) of 4/rev in the non-rotating system of a 4-blade rotor.

TABLE 2 BODY VIBRATION FREQUENCY AND AMPLITUDE CONTENT\*

		ROTOR CONFIGURATION			
Harmonics		4-Blade (6° Twist)	4-blade	3-blade	6-blade
Vertical Vibration	1	33%	33%	16%	30%
	2	14%	neg.	neg.	neg.
	3	neg.	neg.	15%	neg.
	4	14%	25%	neg.	neg.
	5	17%	12%	17%	neg.
	6	20%	15%	20%	50%
	7	neg.	neg.	neg.	neg.
	8	neg.	neg.	13%	neg.
	9	neg.	neg.	neg.	neg.
Longitud. Vibration	1	20%	neg.	neg.	neg.
	2	neg.	neg.	neg.	neg.
	3	neg.	neg.	neg.	neg.
	4	40%	60%	neg.	neg.
	5	neg.	neg.	20%	neg.
	6	neg.	neg.	17%	62%
	7	neg.	neg.	neg.	neg.
	8	20%	neg.	35%	neg.
	9	neg.	neg.	neg.	neg.
Lateral Vibration	1	20%	9%	10%	20%
	2	neg.	neg.	neg.	neg.
	3	neg.	neg.	neg.	neg.
	4	40%	60%	neg.	neg.
	5	neg.	neg.	22%	neg.
	6	neg.	neg.	10%	22%
	7	neg.	neg.	neg.	neg.
	8	20%	12%	30%	20%
	9	neg.	neg.	15%	neg.

\*Percent figures shown are approximate percentages of the total amplitude of the first nine harmonics.



An unusually high 4/rev contribution to the longitudinal and lateral body vibration levels is in all probability due to the near resonant values of the second mode bending chordwise frequency. (Refer to Figure 10). The 4-blade rotor shows half again as much 4/rev as the 4-blade (-6° twist) rotor. This may be due to the effect that angle of attack has on blade frequency. This contention is substantiated by comparison of the mid-chord cyclic stress levels of the 4-blade (-6° twist) configuration to the 4-blade untwisted configuration. The second mode chordwise bending amplitude is lower in the twisted blades. Some vertical 6/rev, which appears in all configurations, is due to the resonance between third mode flap bending frequency and operating r.p.m. (Refer to Figure 10). This 6/rev is much higher in the 3- and 6-blade rotors than in the 4-blade rotors. An 8/rev harmonic term appears in most of the body vibrations for all configurations. This is, as yet, unexplained, but it is believed to be a body component drive system or suspension resonance. This is concluded from its relative lack of sensitivity to number of blades. Some significant 5/rev appears in the vertical body modes of the two 4-blade rotor configurations and all three modes of the 3-blade rotor configuration. This 5/rev is observed in all remaining cases in a lesser magnitude. It is noted that the 5/rev harmonic increased in magnitude in cases in which the 6/rev decreased. It appeared through all cases that the relative contribution of the sum of the 5, 6, and 7/rev tended to stay constant but no explanation of the source of the 5/rev can be offered at the present time.

The 3-blade rotor configuration produced combinations of 3 and 6/rev vibrations. The 3/rev probably results from resonance with second mode flap bending. The 6/rev component is probably due to resonance with third mode flap bending.

The dominant harmonic term of all three body modes for the 6-blade rotor was 6/rev. Although this was the major part of 6-blade rotor configuration body vibration, the magnitude of this vibration was very low.

It should be pointed out here that the resonant or near resonant frequency levels, at operating r.p.m. of second and third mode flap bending, and second mode chordwise bending, shown in Figure 10 are due to the unfortunate stiffening effects of the tungsten wire ballast. The frequency spectrum in Figure 9 represent the actual spectrum that would be associated with a full scale flight article. It is estimated that this spectrum would reduce the body vibration in all configurations through better avoidance of blade natural frequencies at operating r.p.m.

Figures 41 through 52 show that vibration levels stay relatively constant with forward speed. The body vibration tends to increase with load factor, but the increase is not large.

## CONCLUSIONS AND RECOMMENDATIONS

The fundamental conclusion to be drawn from this program is the matched-blade/flexure-hub type of rigid rotor is a workable concept capable of further advancing the helicopter state of the art. The following advantages of this type of rotor were demonstrated:

1. Rotor stability with a very small gyro.
2. Extremely small control force requirements.
3. Elimination of feathering bearings.

The ground-air resonance phenomenon was produced and eliminated and was in general found to be predictable and preventable by the separation of frequencies without the need to complicate the hub with dampers, etc.

Inasmuch as the scaling laws indicate that the test results can be applied to any size rotor, there is no inherent size limitation to this type of rotor. The only question not resolved is the exact weight of large matched-blade/flexure-hub rotors. In Figure 22 an attempt is made based on some limited studies of large flex-hub rotors to project the model (and simulated vehicle) rotor weights to large diameters. The information gained from this program allows the design of lighter rotors than was anticipated. Thus, the simulated rotor, designed at the beginning of the program, falls above the band of projected flex-hub rotor weights.

It is recommended that research in this new and promising field of rigid-rotor design be pursued in the following ways:

1. A 35-foot-diameter matched-blade/flexure-hub rotor be built and flight tested on an XH-51 helicopter to obtain a flight evaluation of this new concept and a comparison with the chord-stiff type of rigid rotor.
2. A detailed design study of an approximately 100-foot-diameter matched-blade/flexure-hub rotor be executed to obtain accurate weight information on large rotors of this type.

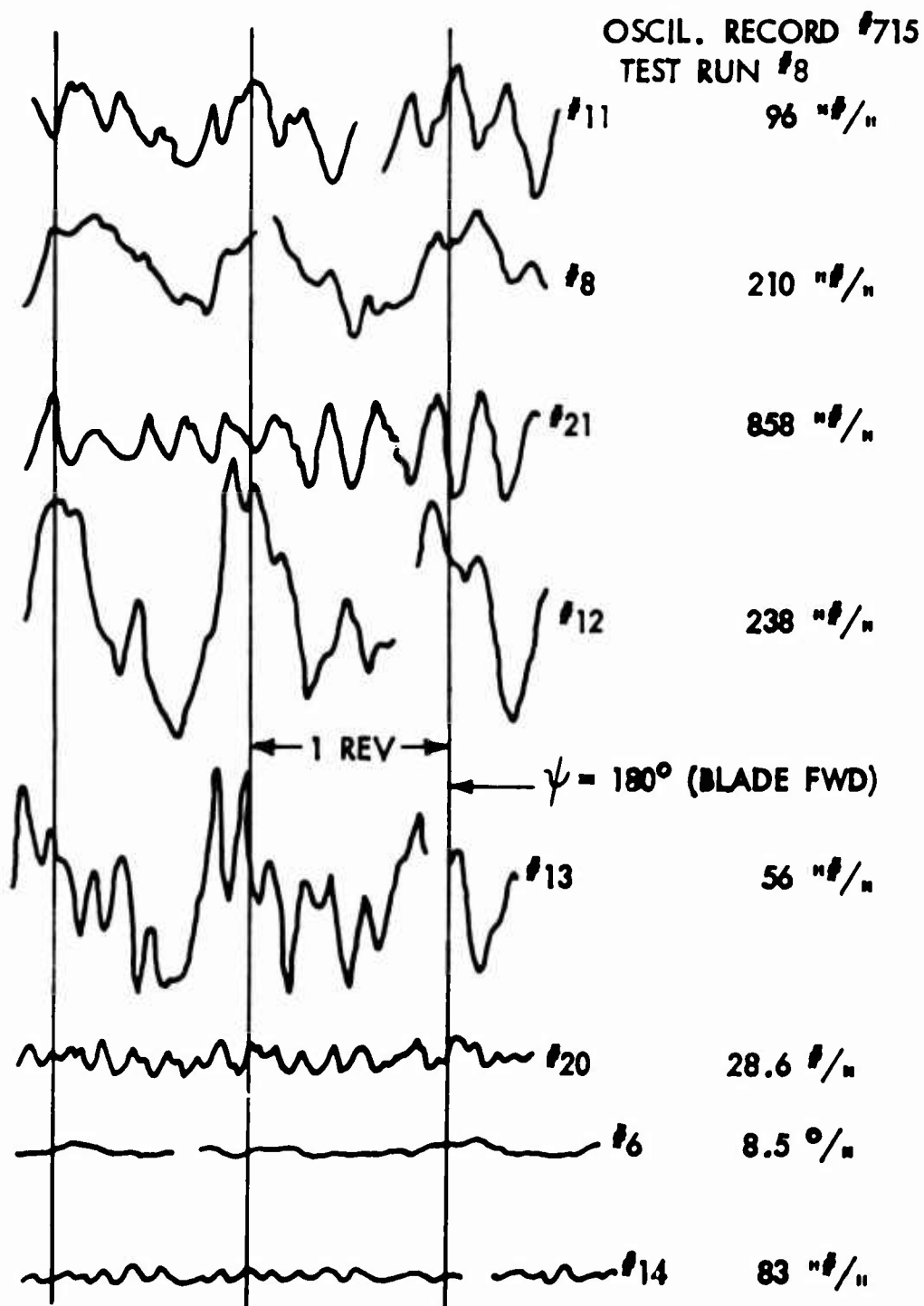


FIG. 13 - 4-BLADE ROTOR LOADS, 1.5 "g", 0 MPH



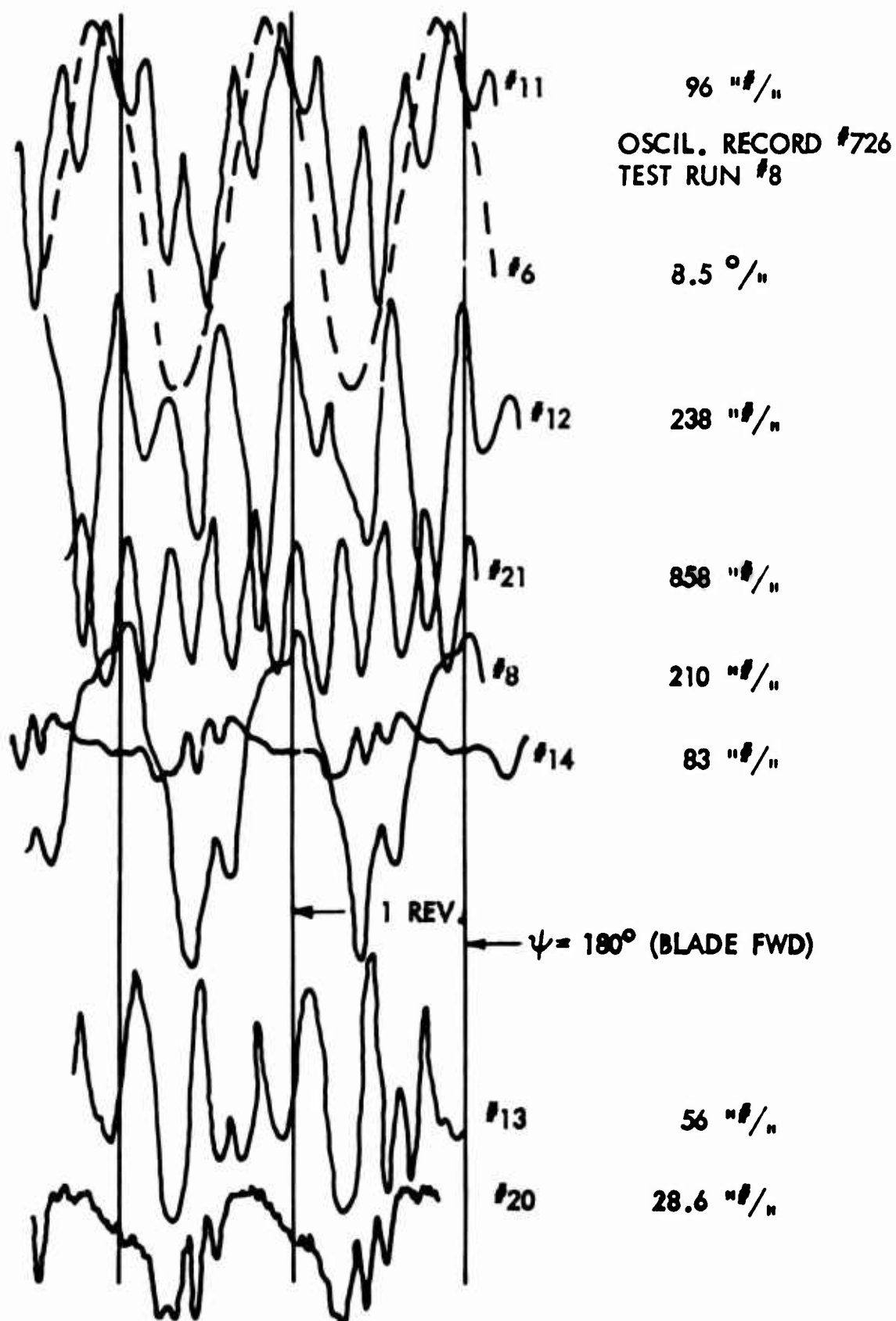


FIG. 14 - 4-BLADE ROTOR LOADS, 1.25 "g", 100 MPH

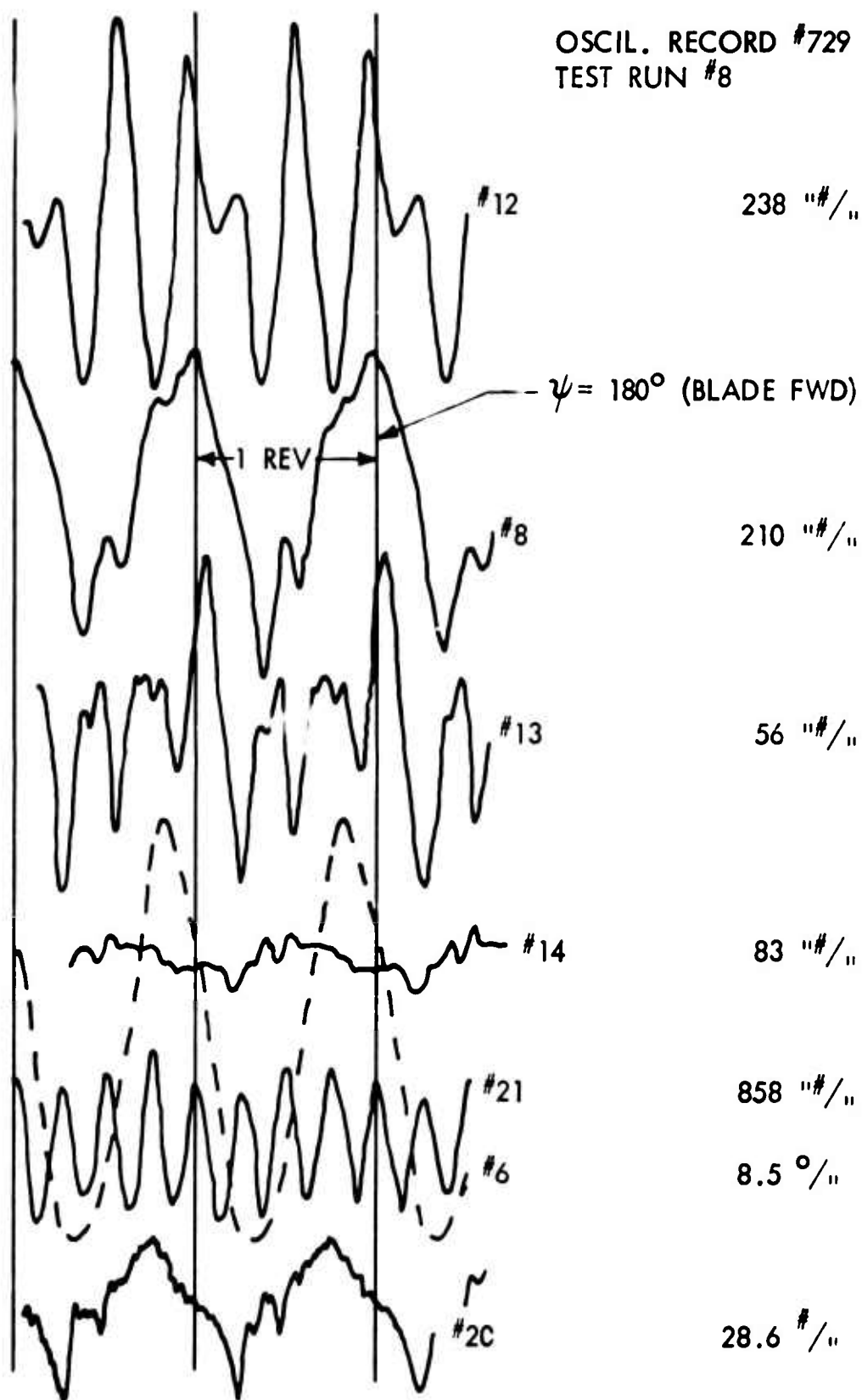


FIG. 15 - 4-BLADE ROTOR LOADS, 1.0 "g", 140 MPH

OSCIL. RECORD #742  
TEST RUN #8

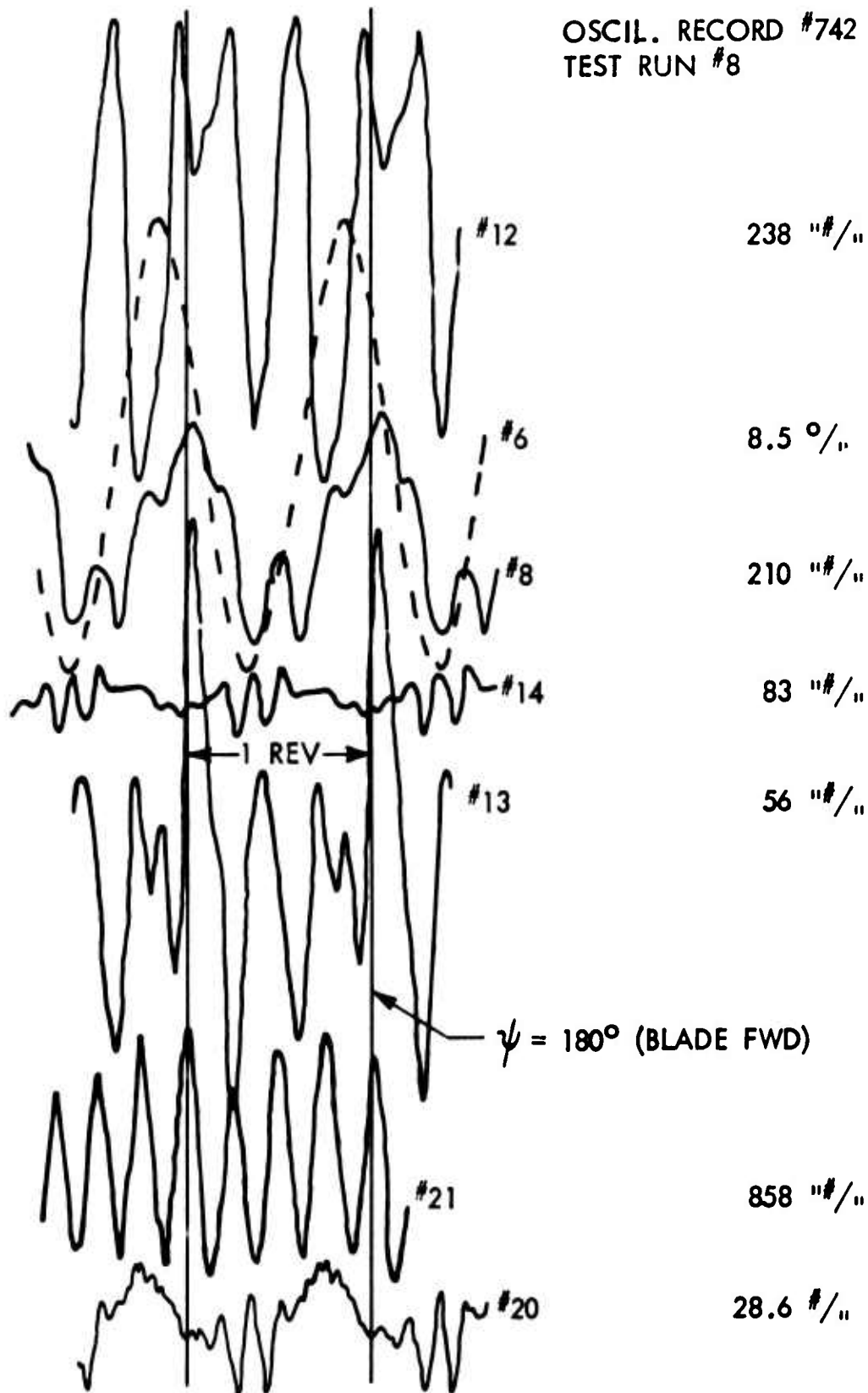


FIG. 16 - 4-BLADE ROTOR LOADS, .75 "g", 200 MPH

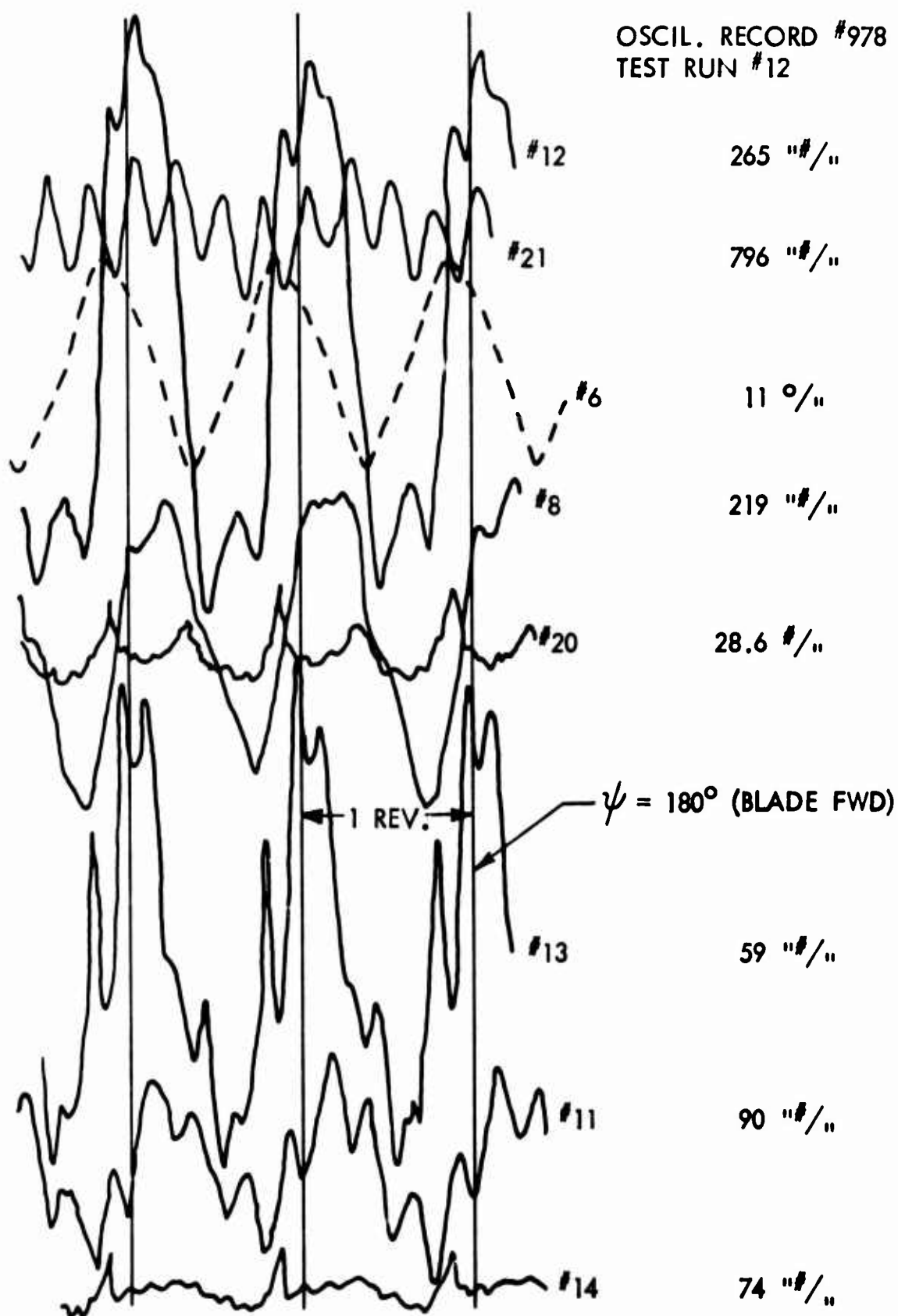


FIG. 17 - 4-BLADE ROTOR LOADS, 0 "g", 250 MPH

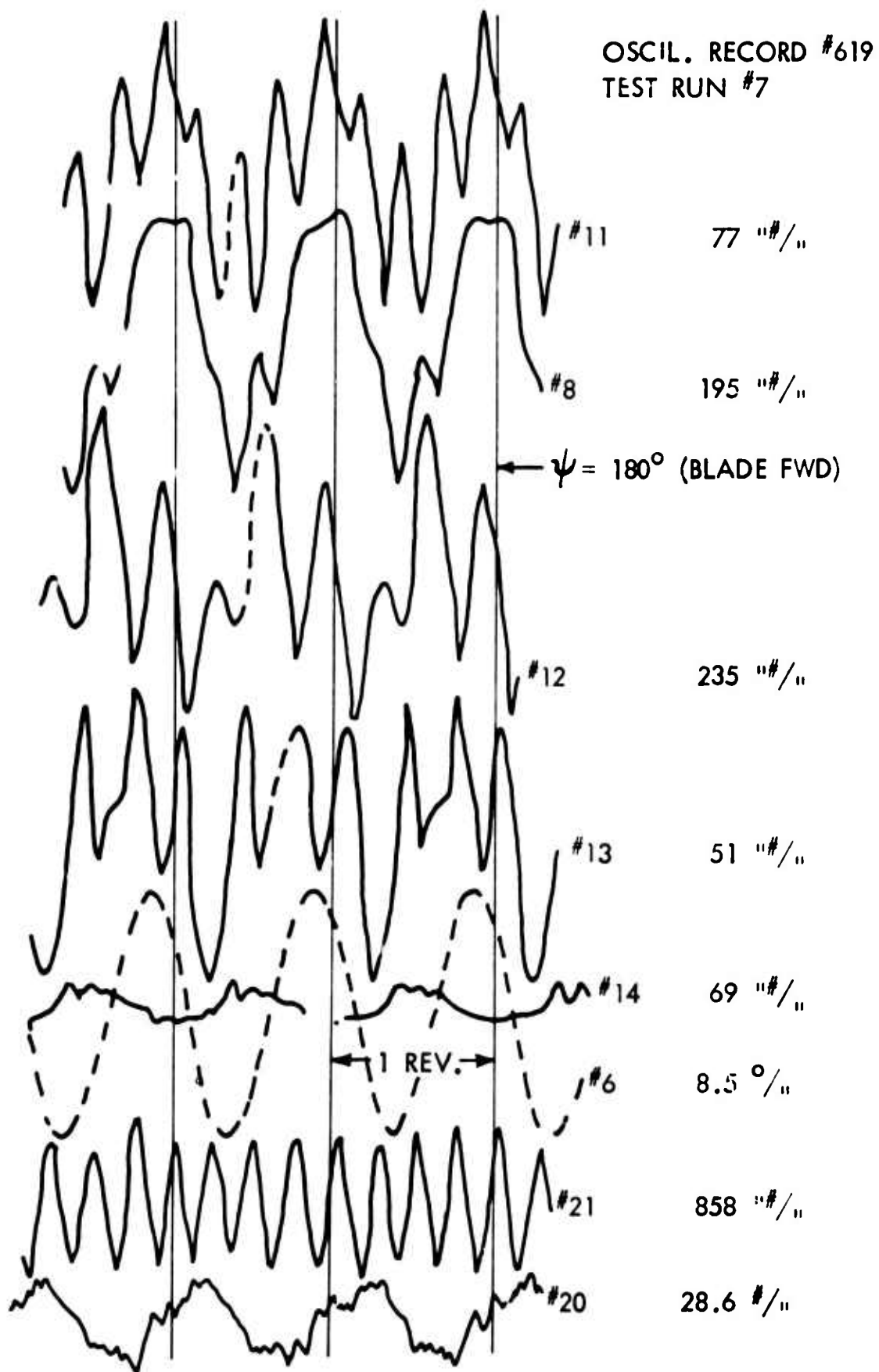


FIG. 18 - TWISTED BLADE LOADS, 1.3 "g", 100 MPH

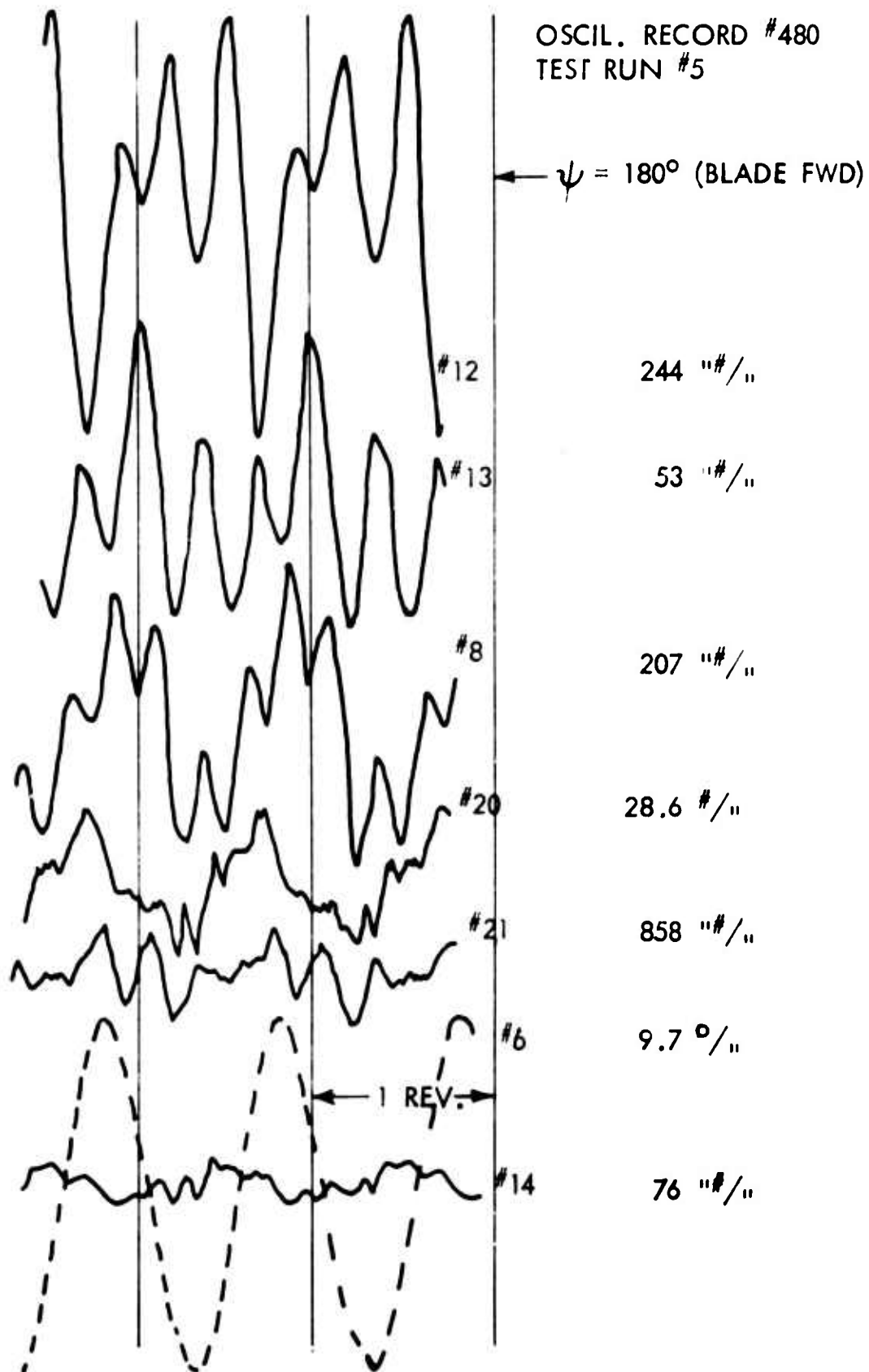


FIG. 19 - 3-BLADE ROTOR LOADS, .65 "g", 140 MPH

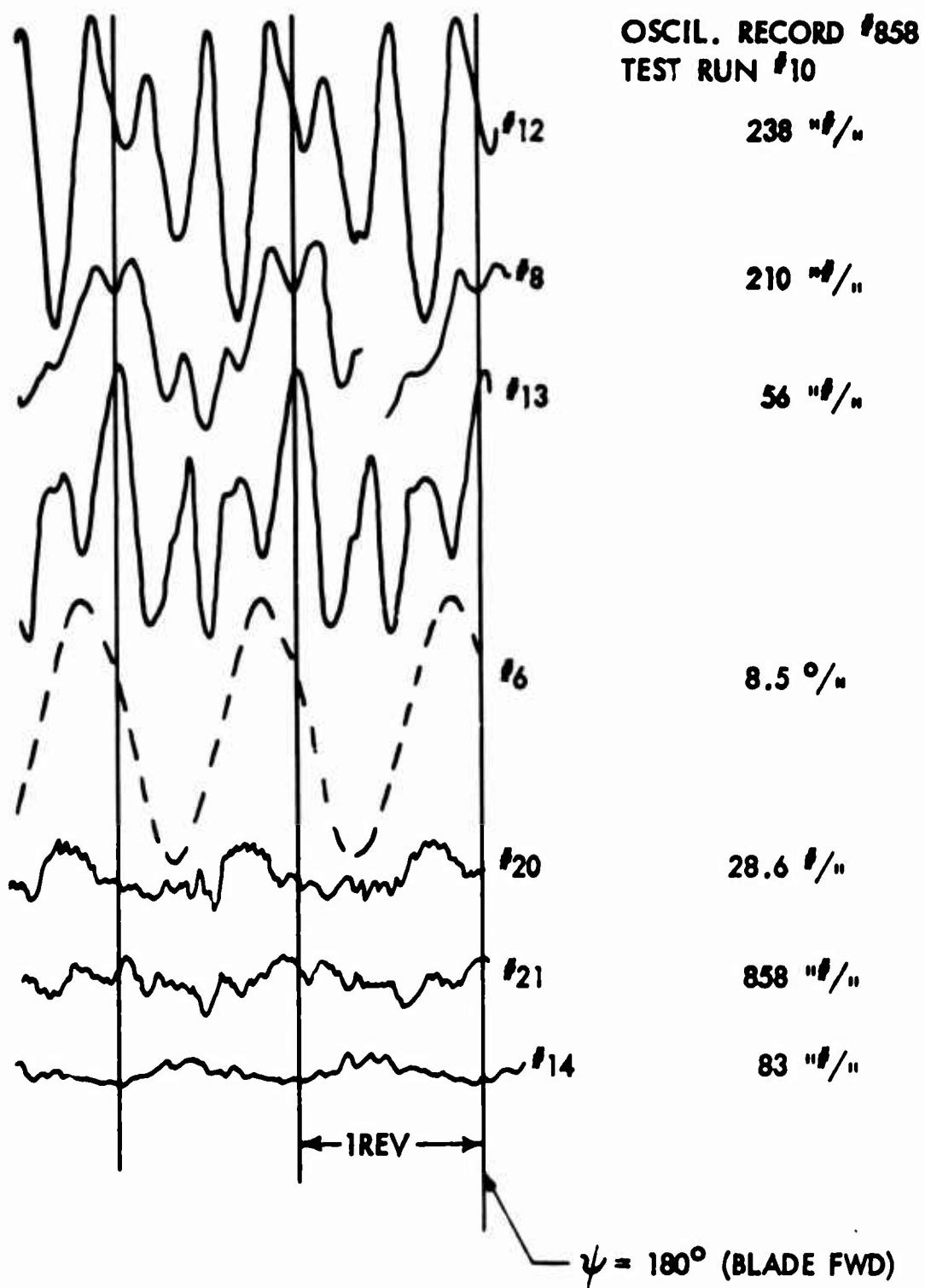


FIG. 20 - 6-BLADE ROTOR LOADS, 1.25 "g", 140 MPH

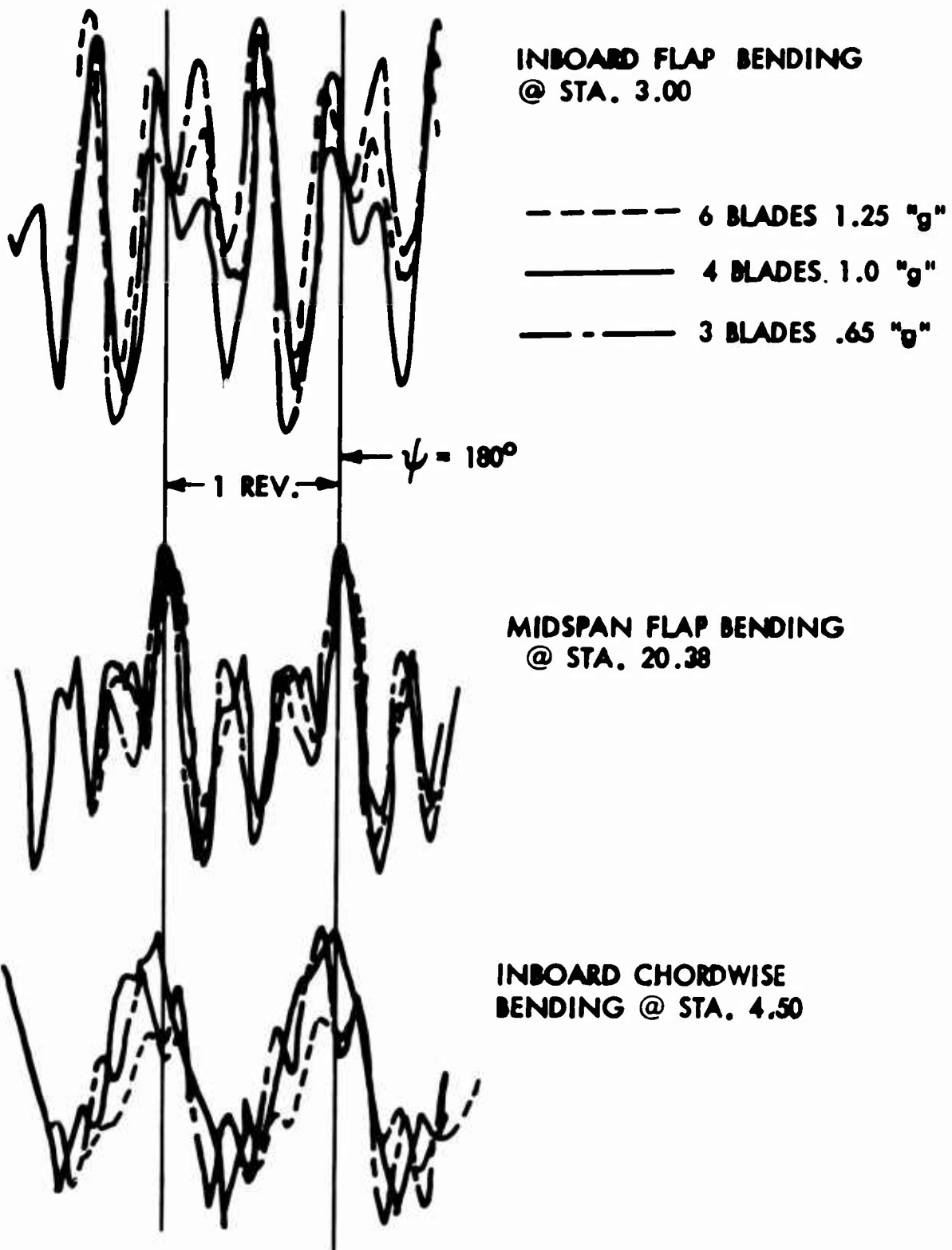


FIG. 21 - 3-, 4-, & 6-BLADE LOAD COMPARISONS AT 140 MPH



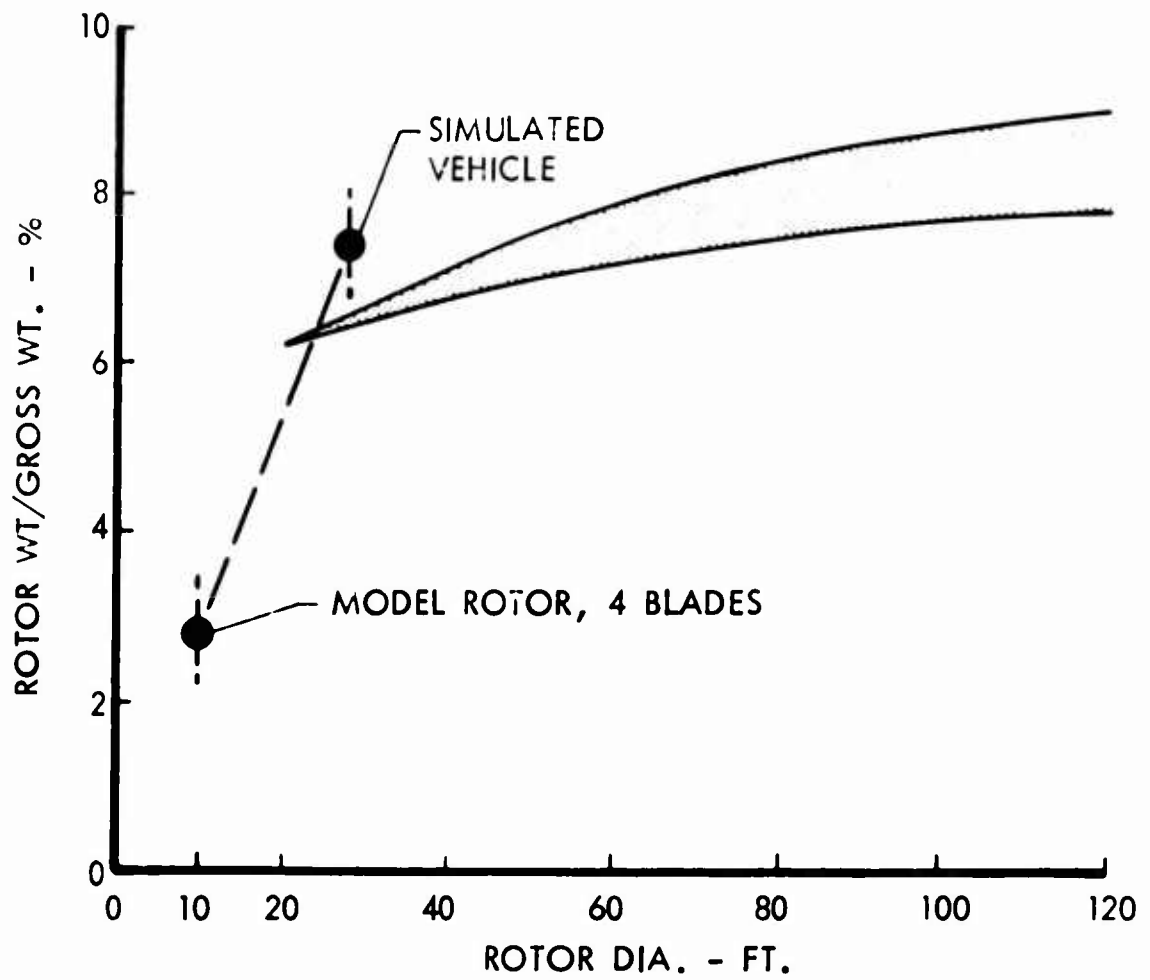


FIG. 22 - FLEXURE HUB ROTOR WEIGHT TRENDS

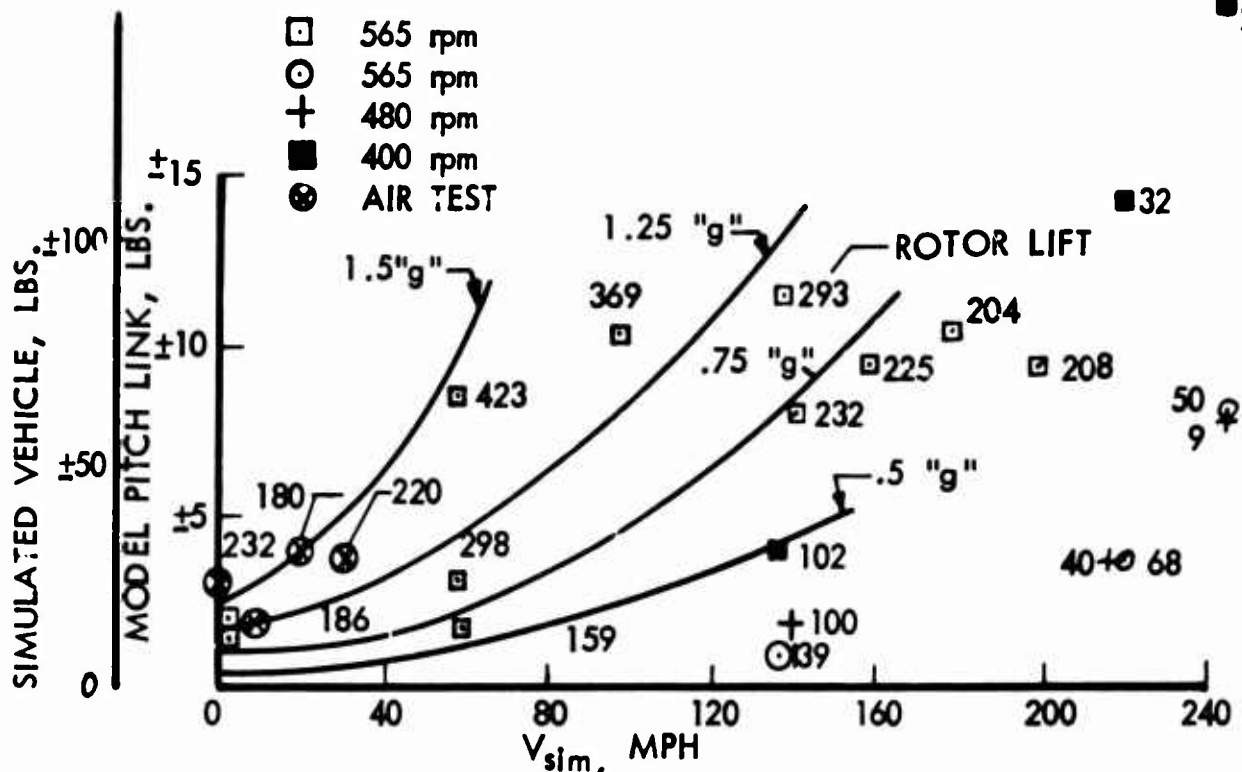


FIG. 23 - FWD. SPEED VS OSCILLATING PITCH LINK LOAD, 4-BLADE ROTOR

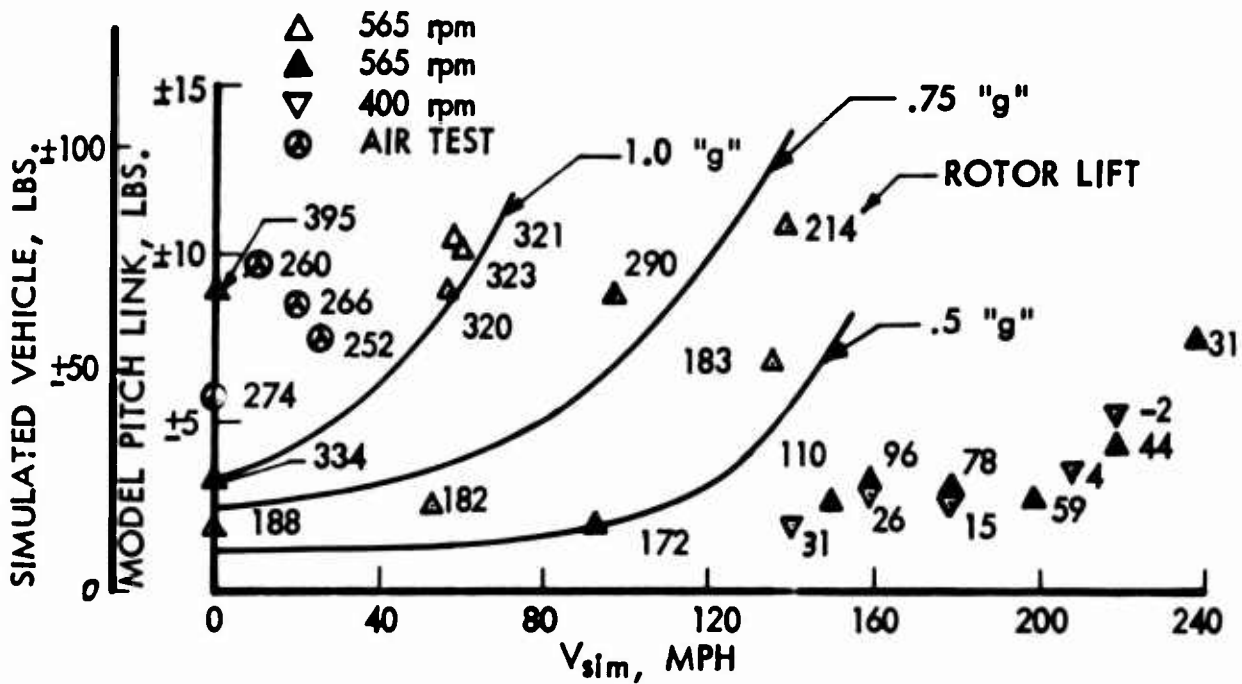


FIG. 24 - FWD. SPEED VS OSCILLATING PITCH LINK LOAD, 3-BLADE ROTOR

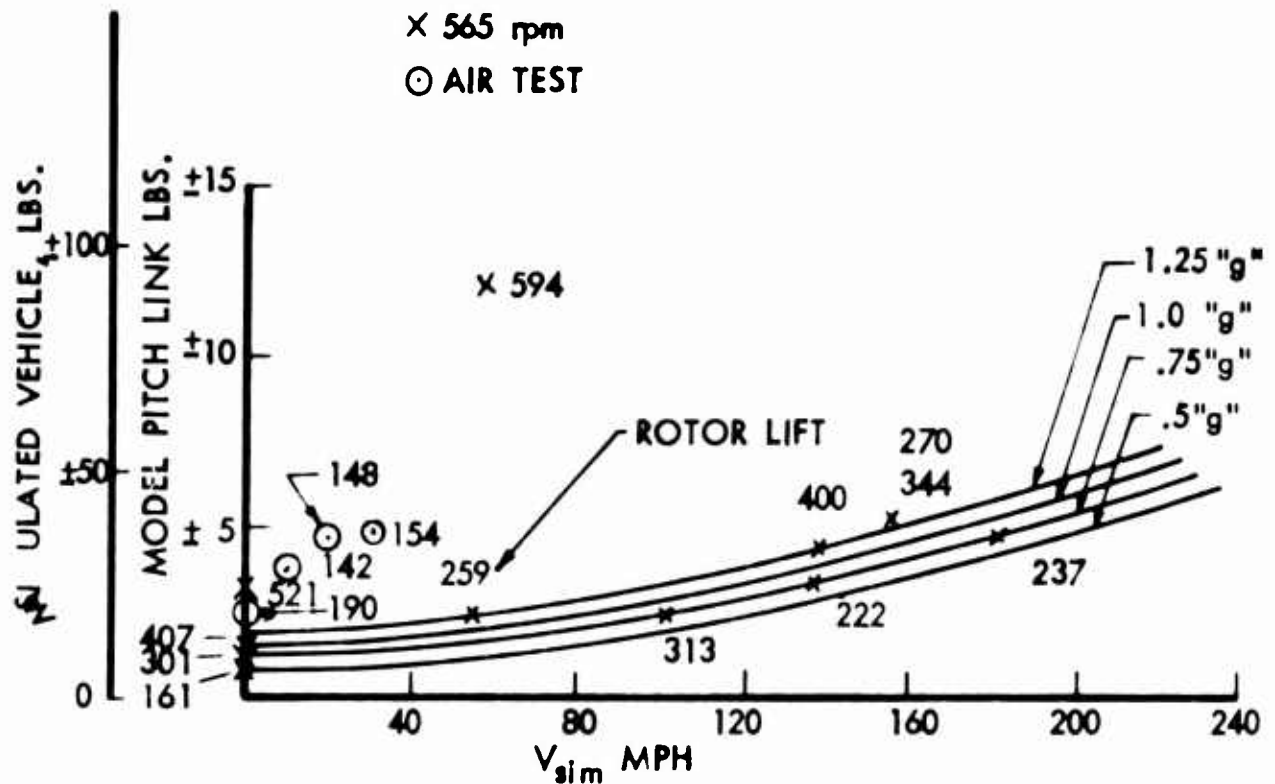


FIG. 25 - FWD. SPEED VS OSCILLATING PITCH LINK LOAD, 6-BLADE ROTOR

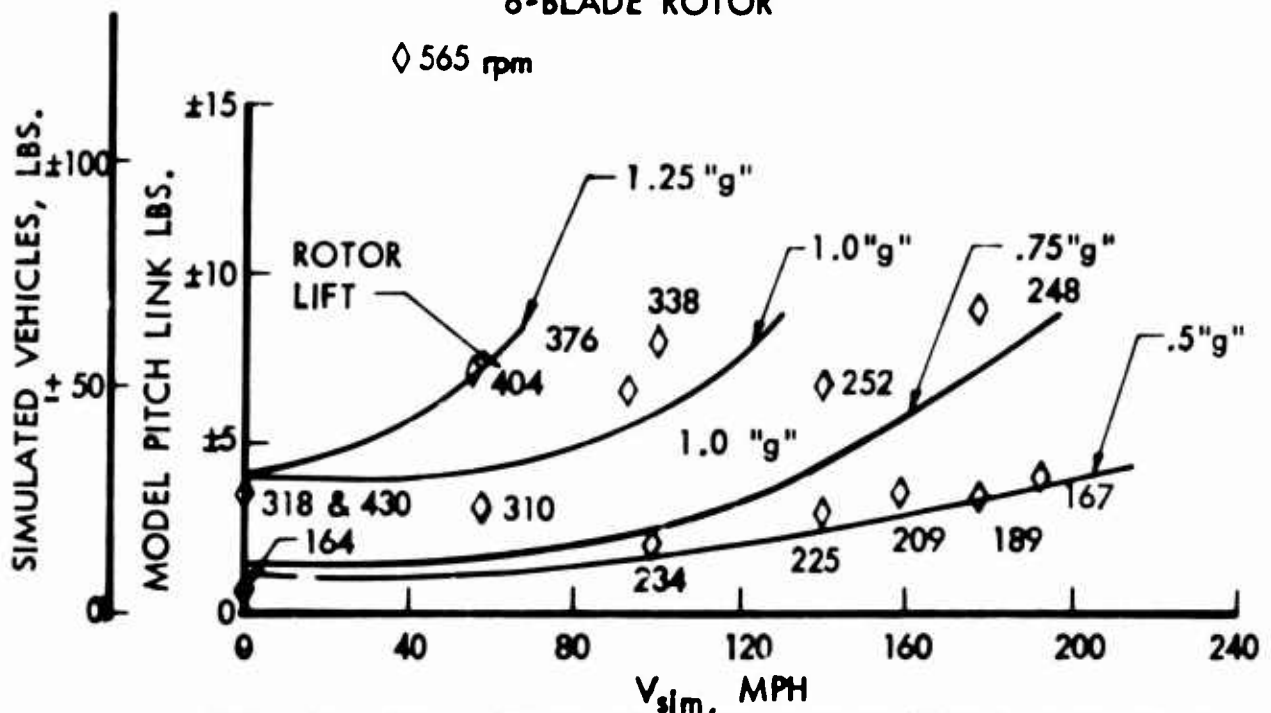


FIG. 26 - FWD. SPEED VS OSCILLATING PITCH LINK LOAD, 4-BLADE ( $-6^\circ$  TWIST) ROTOR

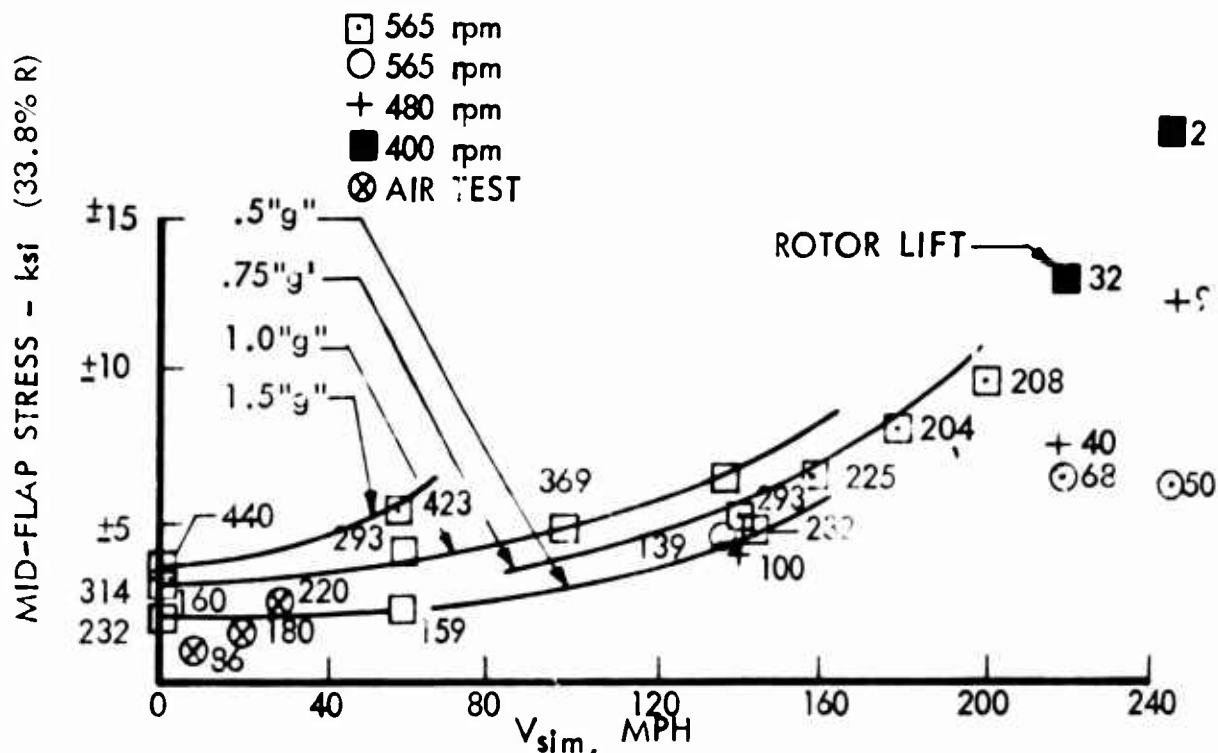


FIG. 27 - FWD. SPEED VS MID-FLAP CYCLIC STRESS, 4-BLADE ROTOR

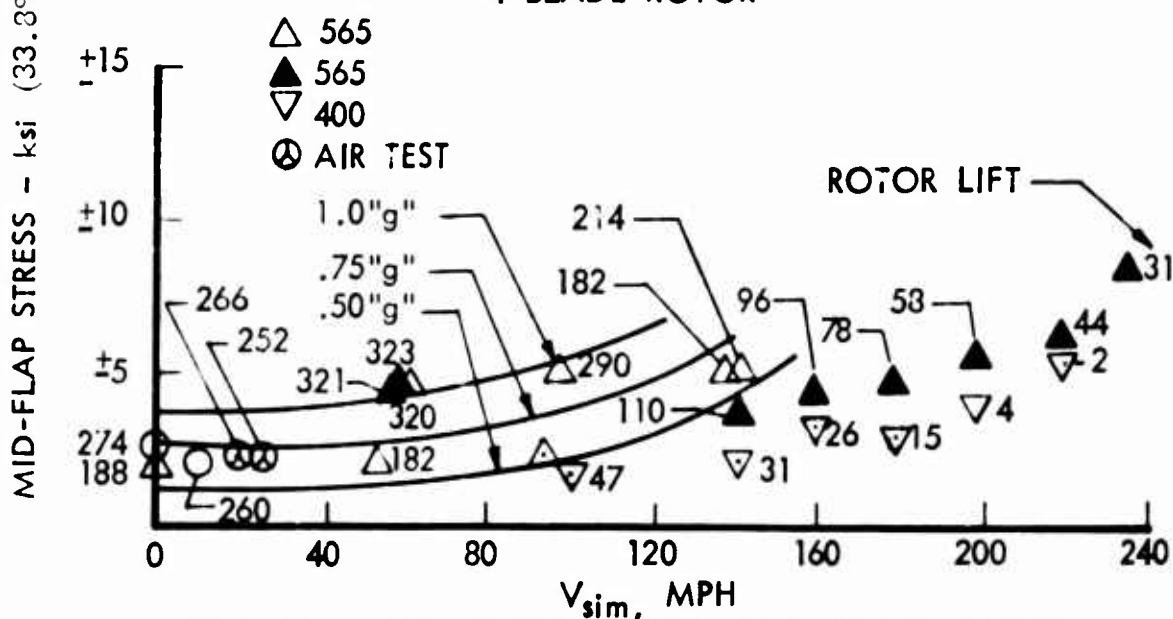


FIG. 28 - FWD. SPEED VS MID-FLAP CYCLIC STRESS, 3-BLADE ROTOR

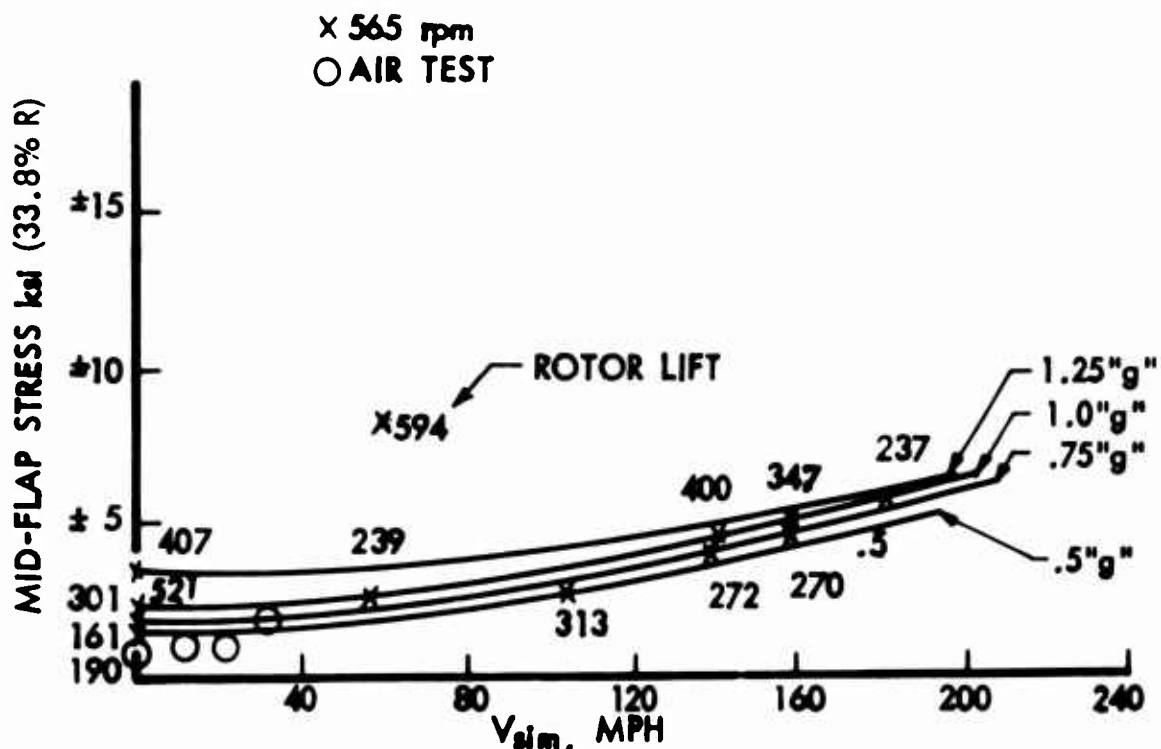


FIG. 29 - FWD. SPEED VS MID-FLAP CYCLIC STRESS, 6-BLADE ROTOR

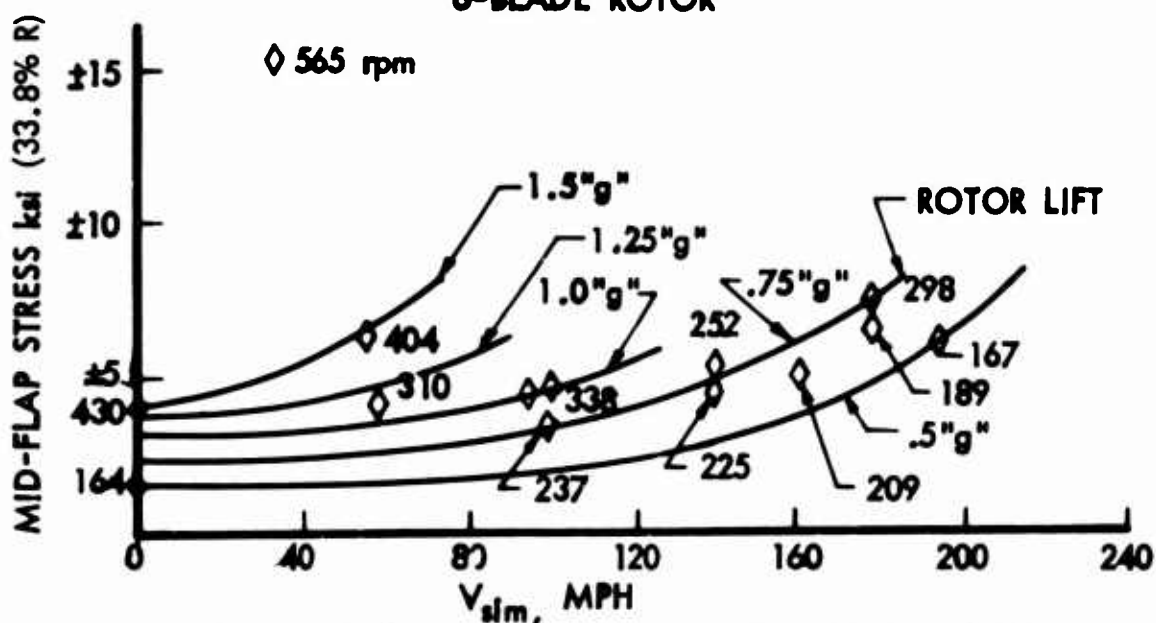


FIG. 30 - FWD. SPEED VS MID-FLAP CYCLIC STRESS, 4-BLADE (-6° TWIST) ROTOR

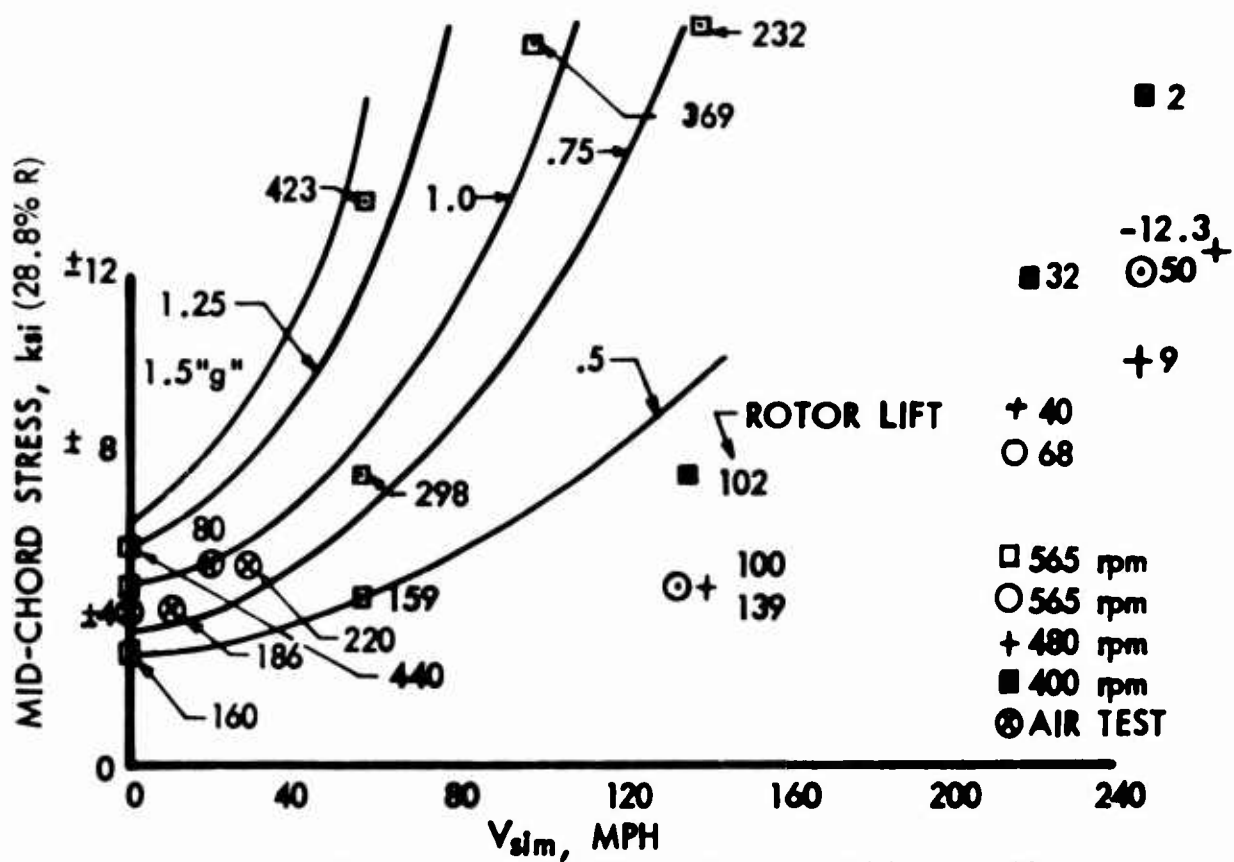


FIG. 31 - FWD. SPEED VS MID-CHORD CYCLIC STRESS, 4-BLADE ROTOR

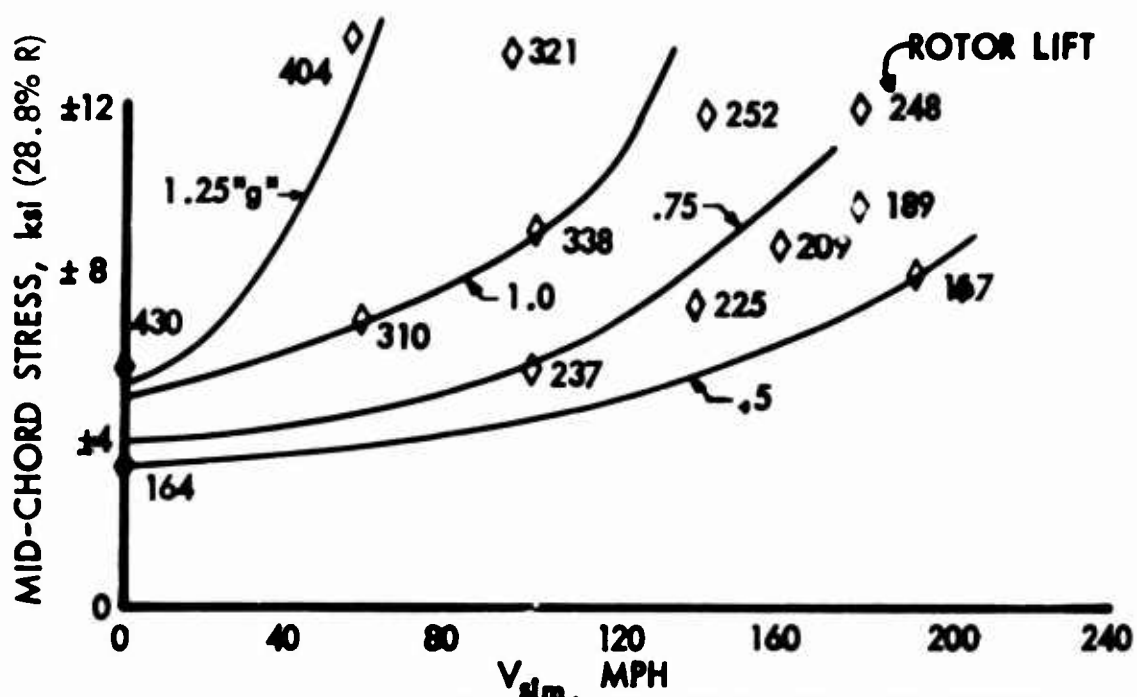


FIG. 32 - FWD. SPEED VS MID-CHORD CYCLIC STRESS, 4-BLADE (-6° TWIST) ROTOR

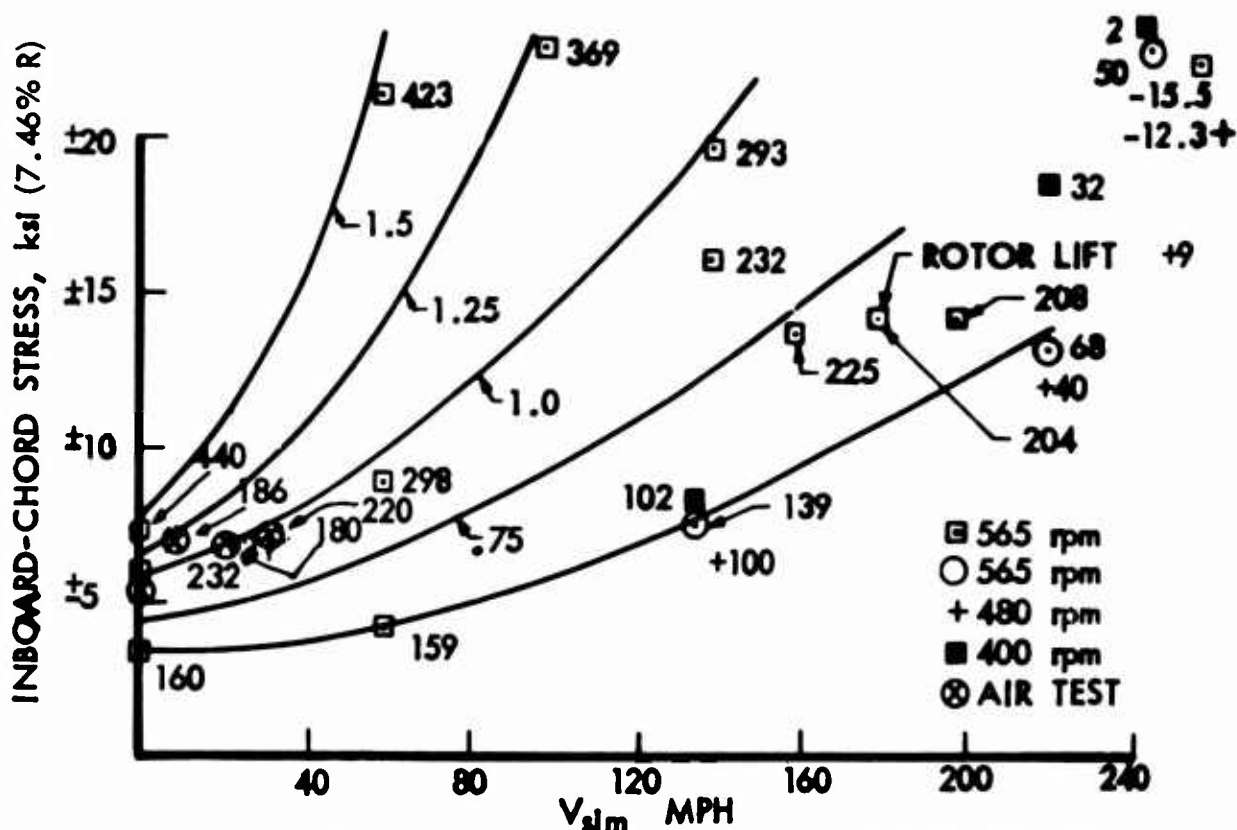


FIG. 33 - FWD SPEED VS INBOARD CHORD CYCLIC STRESS,  
4-BLADE ROTOR

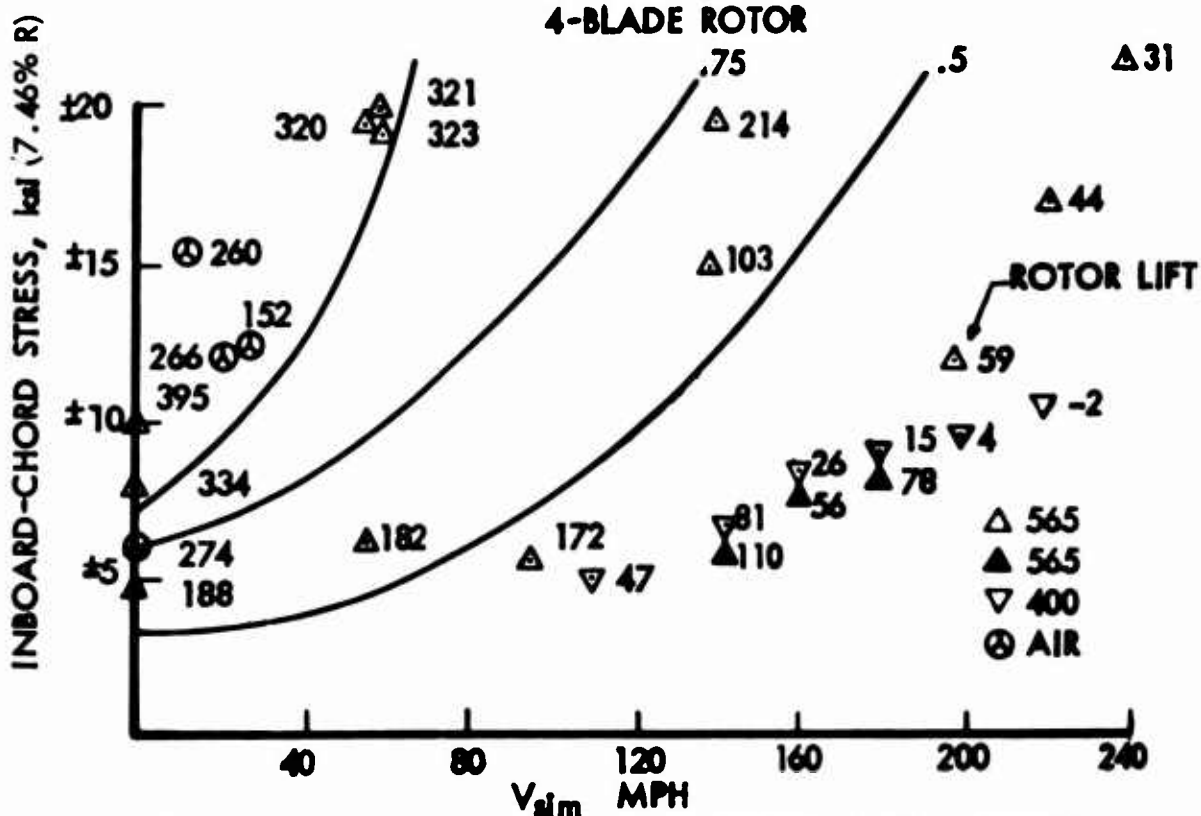


FIG. 34 - FWD SPEED VS INBOARD CHORD CYCLIC STRESS,  
3-BLADE ROTOR

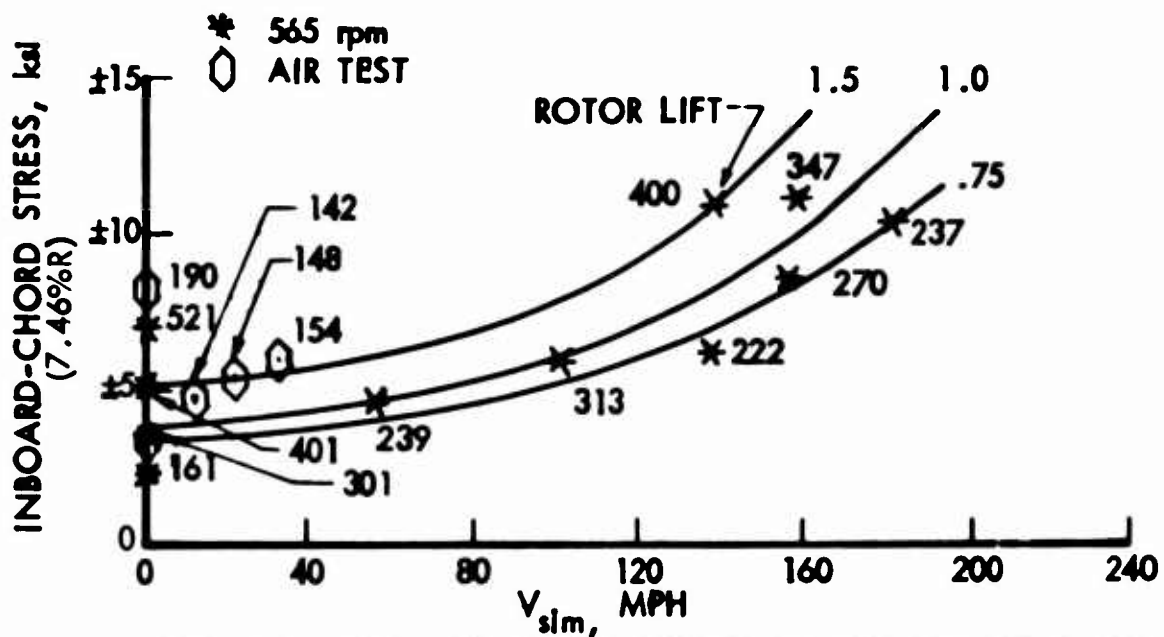


FIG. 35 - FWD. SPEED VS INBOARD-CHORD CYCLIC STRESS, 6 BLADE ROTOR

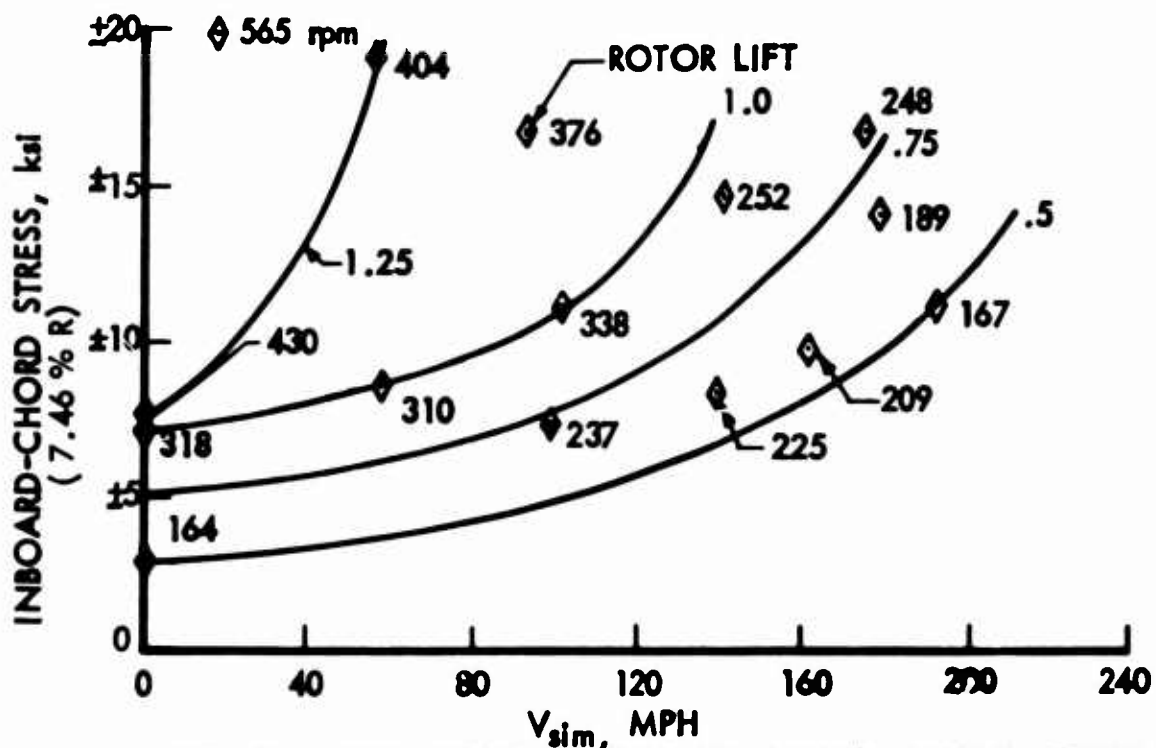
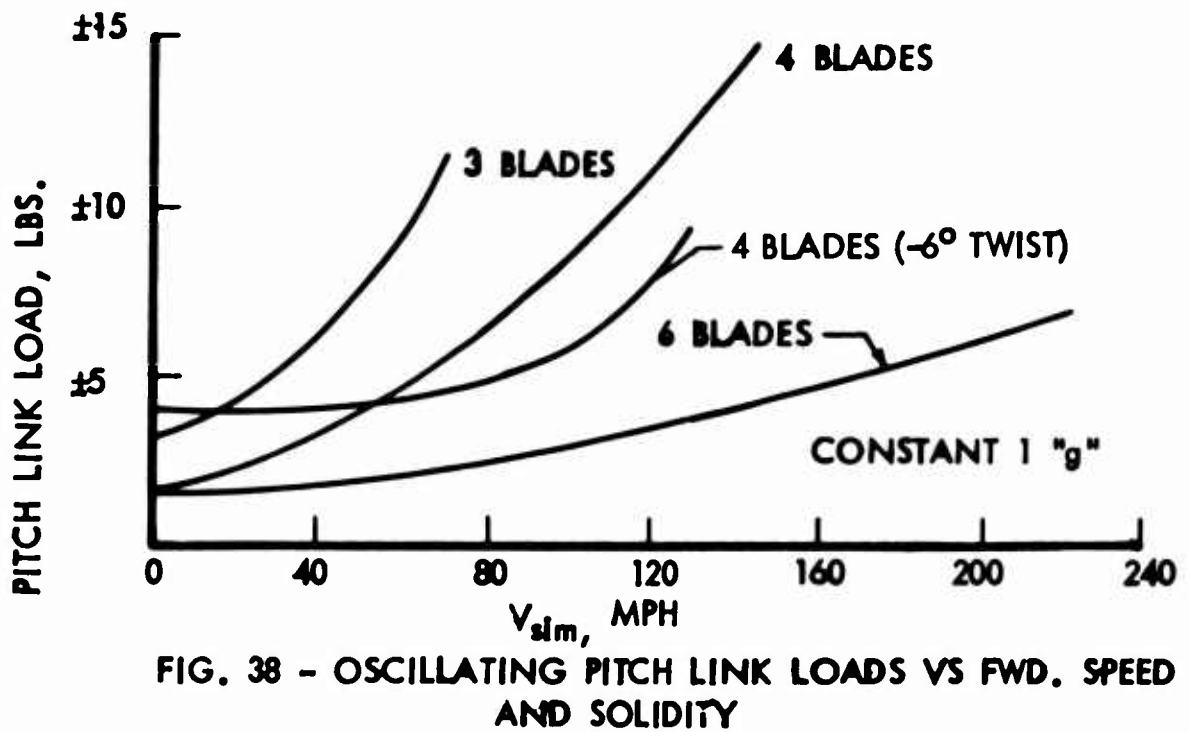
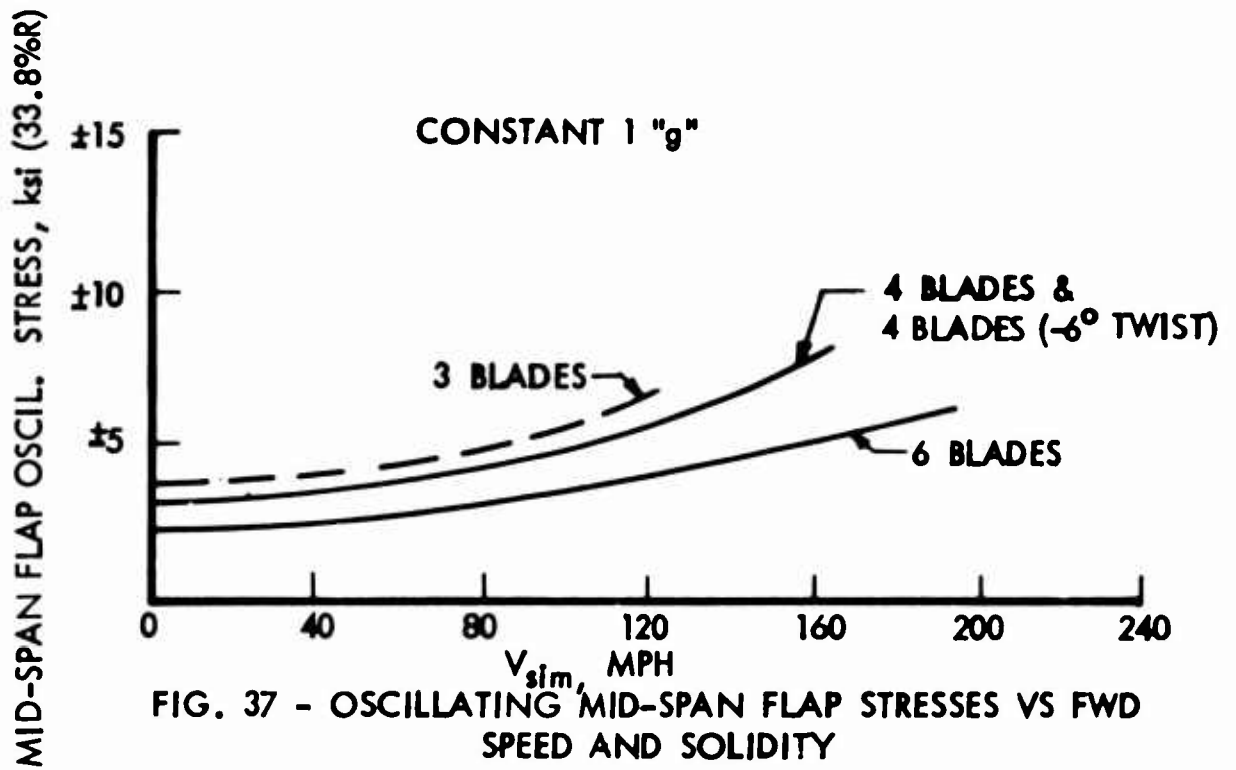


FIG. 36 - FWD SPEED VS INBOARD-CHORD CYCLIC STRESS, 4- BLADE (-6° TWIST) ROTOR





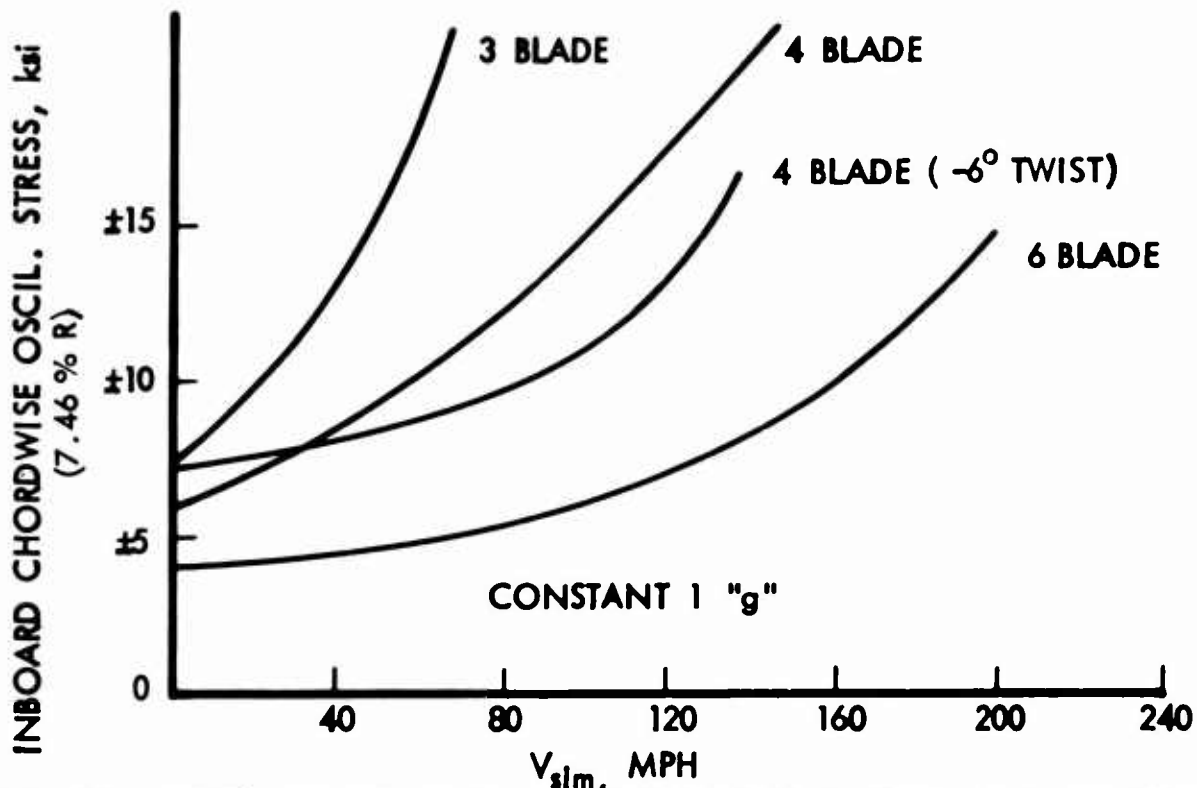


FIG. 39 - OSCILLATING IN-PLANE STRESS VS FWD SPEED AND SOLIDITY

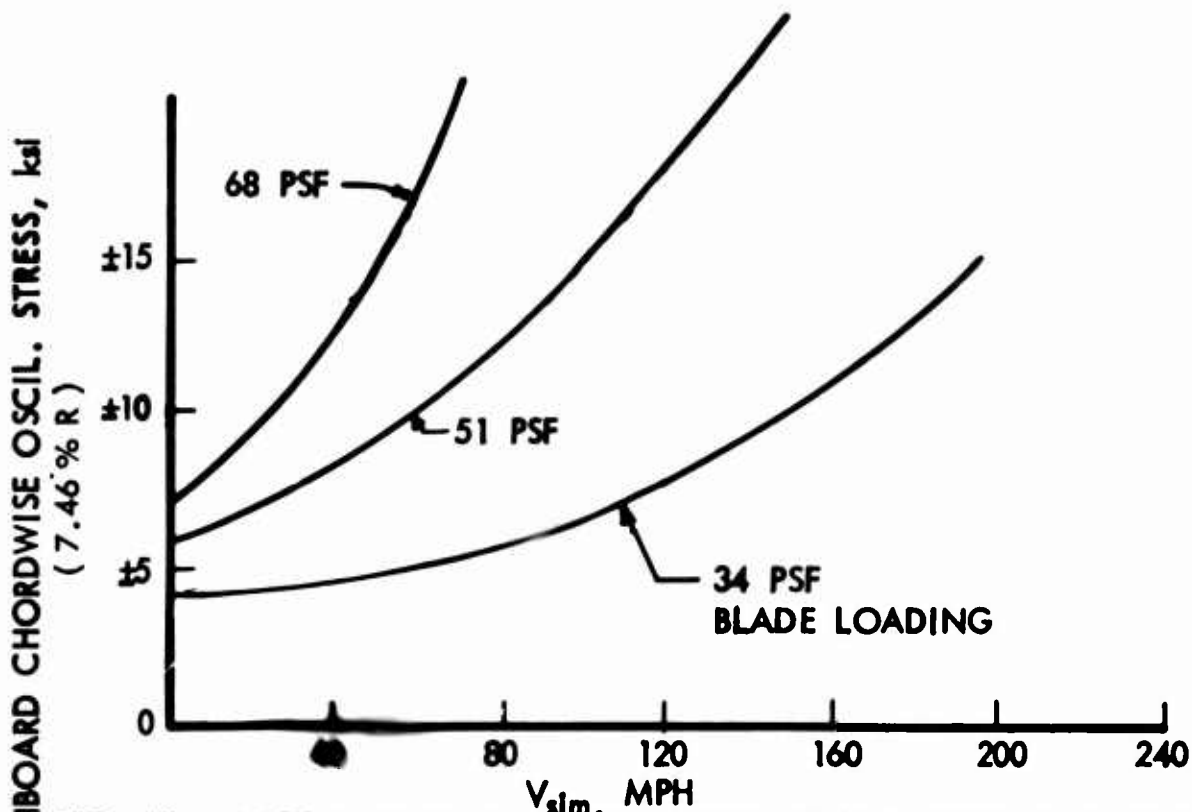


FIG. 40 - OSCILLATING IN-PLANE STRESS VS FWD SPEED AND BLADE LOADING

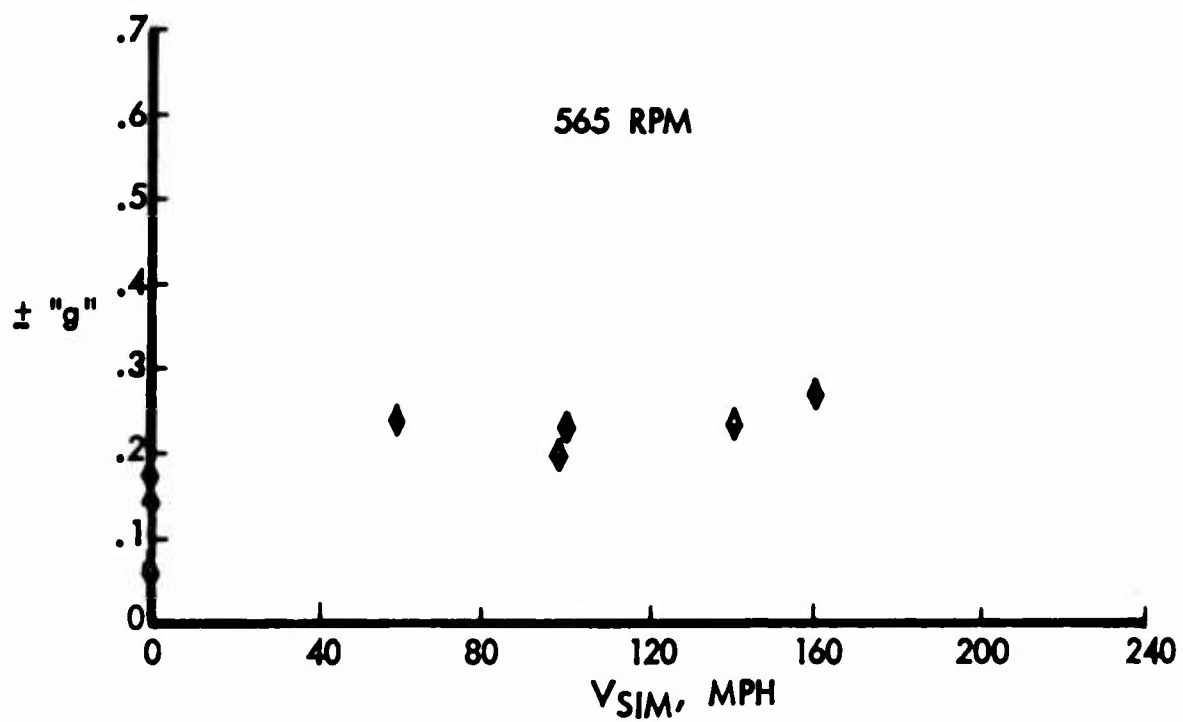


FIG. 41 - VERTICAL BODY VIBRATION VS FWD. SPEED, 4-BLADE (-6°TWIST) ROTOR

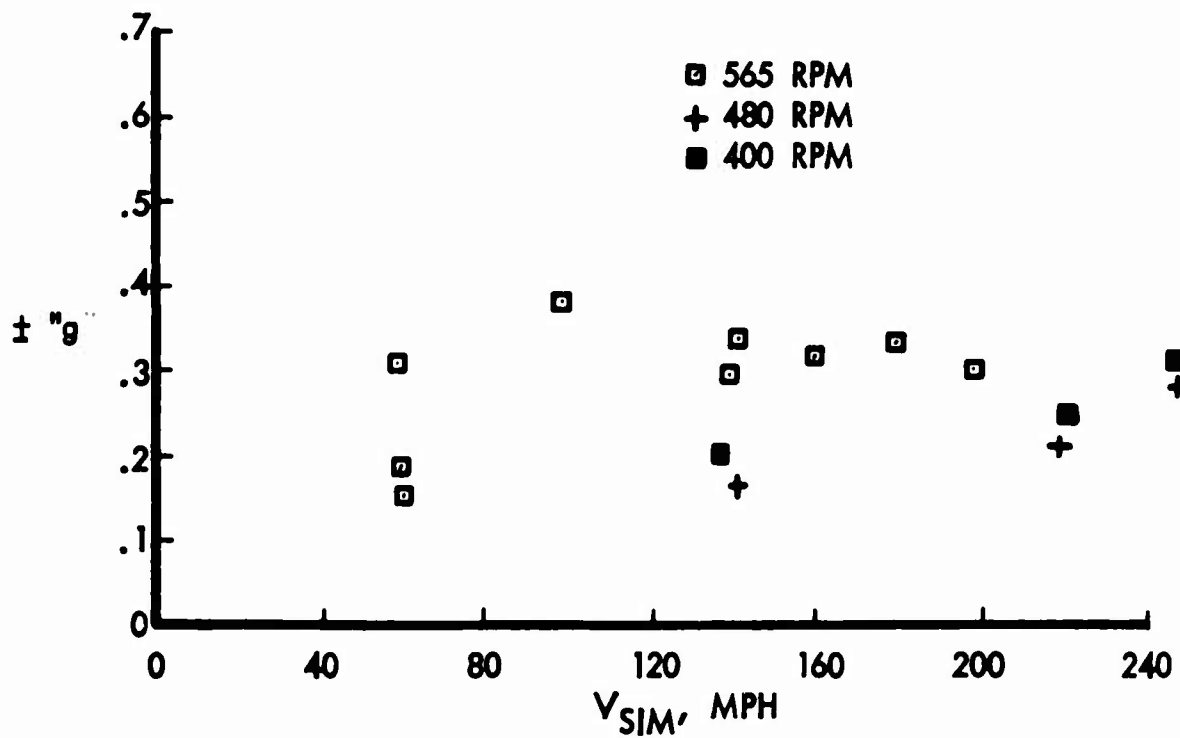


FIG. 42 - VERTICAL BODY VIBRATION VS FWD. SPEED, 4-BLADE ROTOR

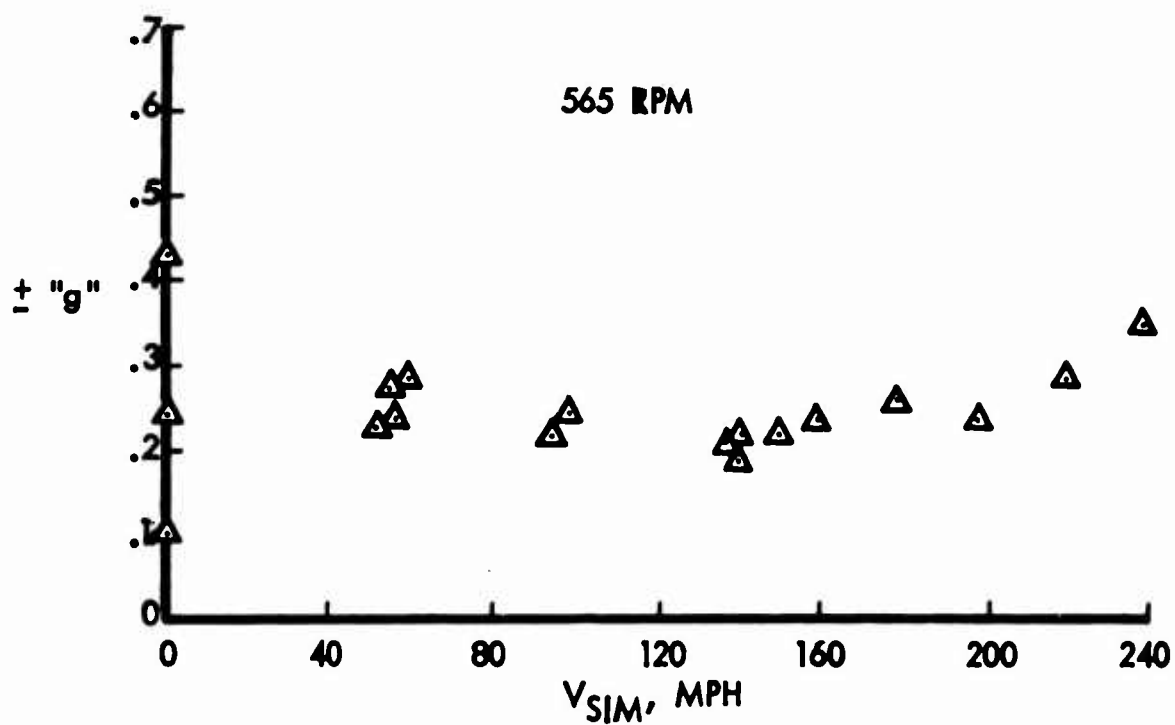


FIG. 43 - VERTICAL BODY VIBRATION VS FWD. SPEED, 3-BLADE ROTOR

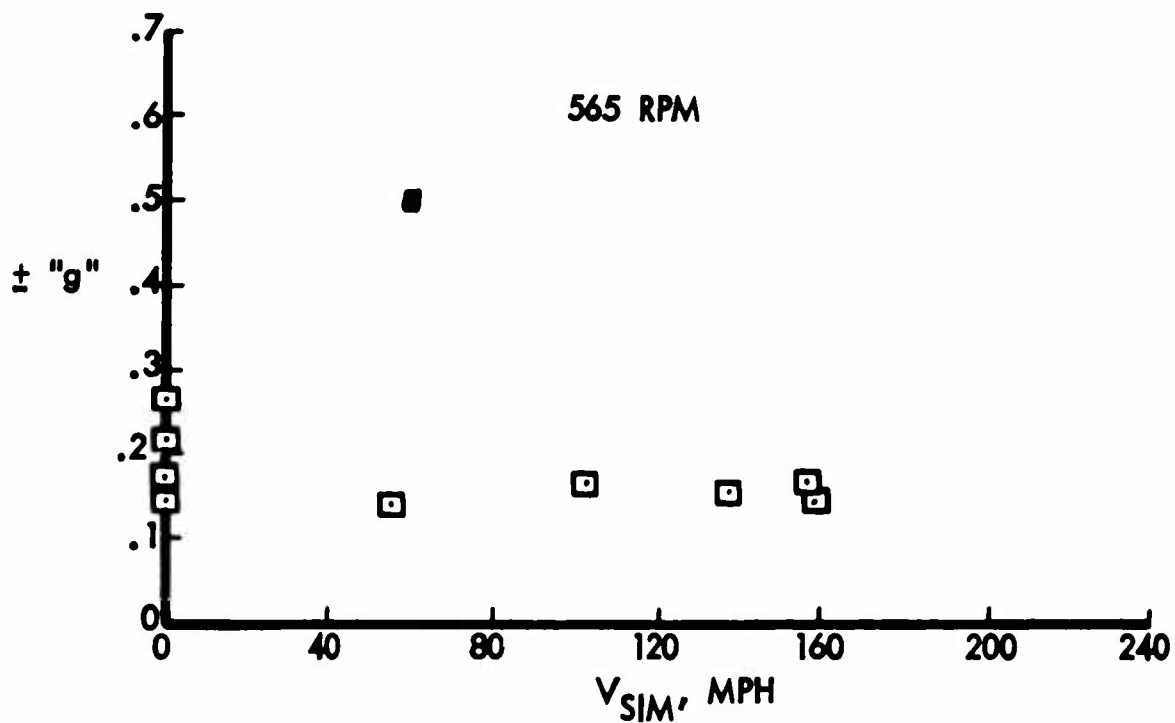


FIG. 44 - VERTICAL BODY VIBRATION VS. FWD. SPEED, 6-BLADE ROTOR

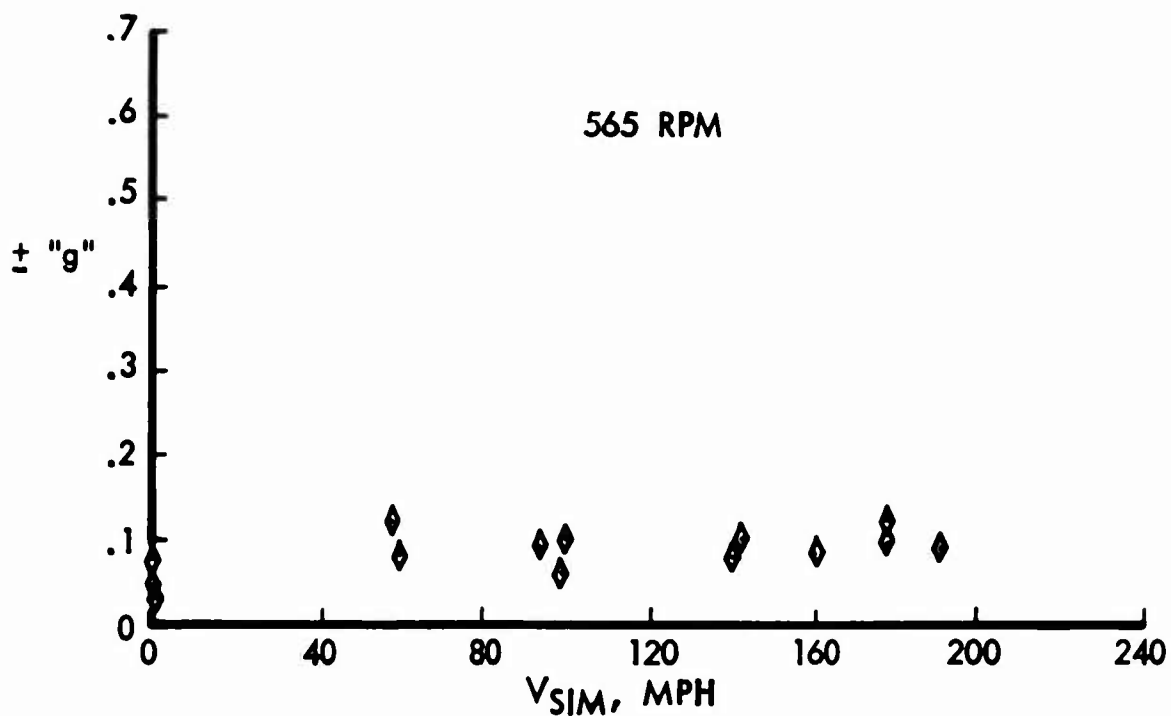


FIG. 45 - LONGITUDINAL BODY VIBRATION VS FWD. SPEED, 4-BLADE ( $-6^\circ$  TWIST) ROTOR

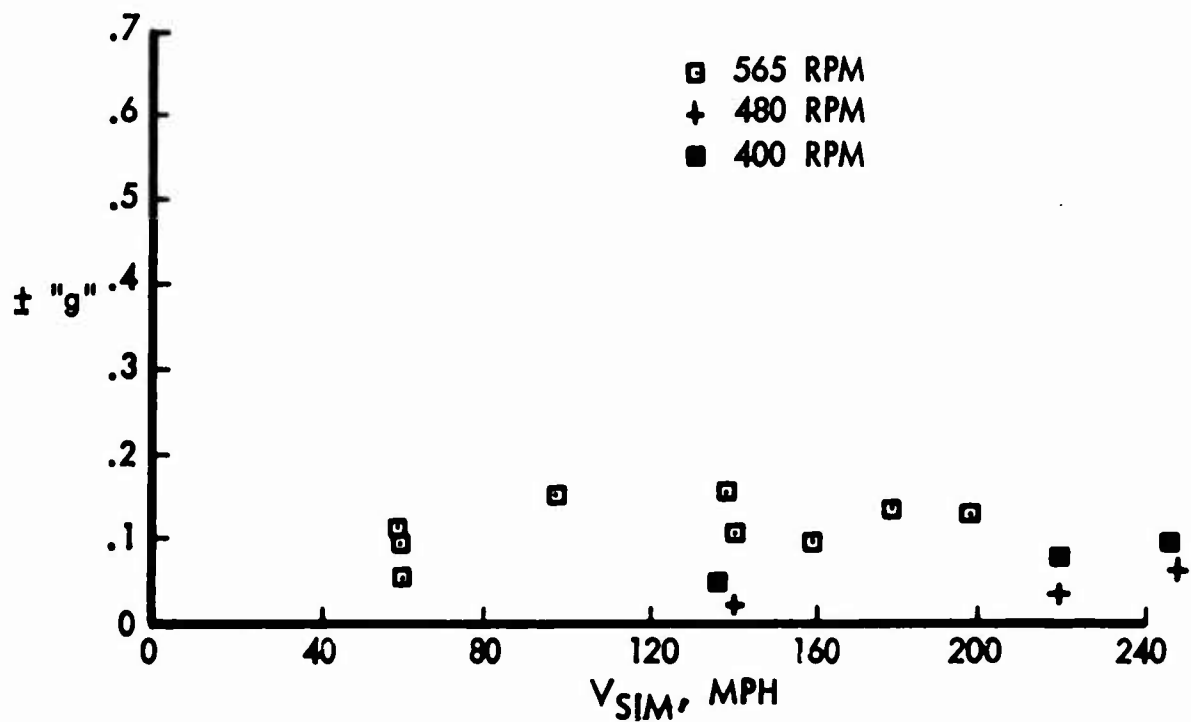


FIG. 46 - LONGITUDINAL BODY VIBRATION VS FWD. SPEED, 4-BLADE ROTOR

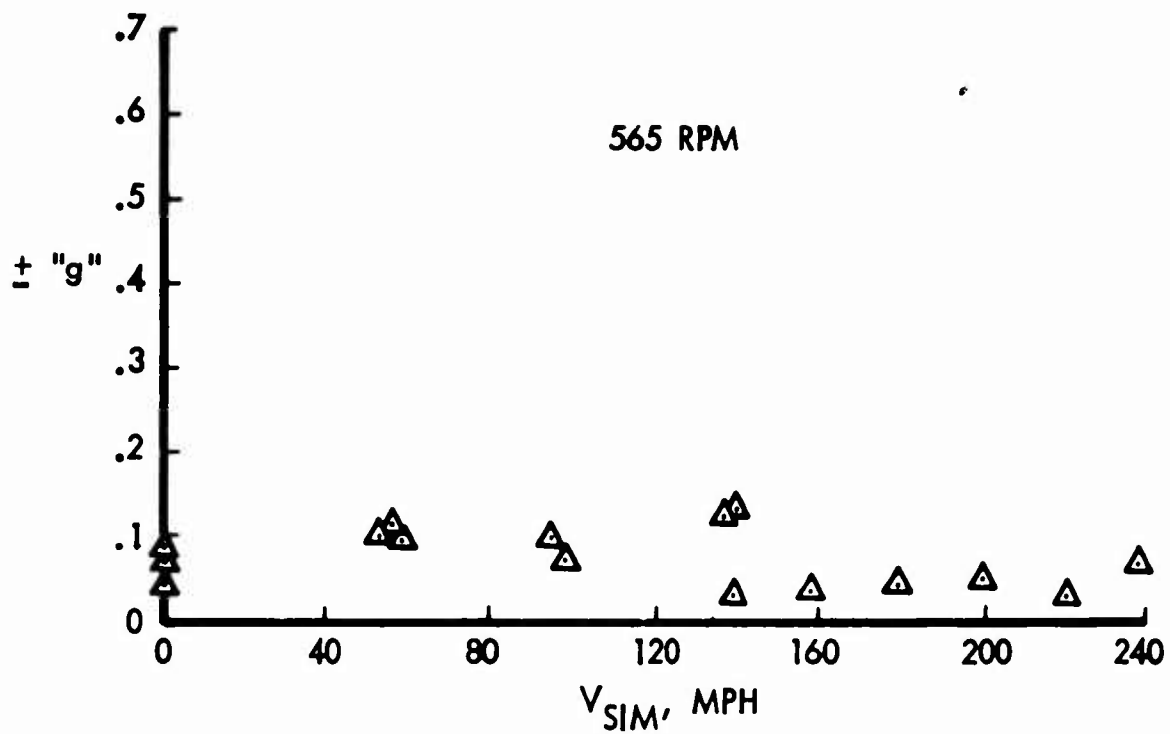


FIG. 47 - LONGITUDINAL BODY VIBRATION VS FWD. SPEED, 3-BLADE ROTOR

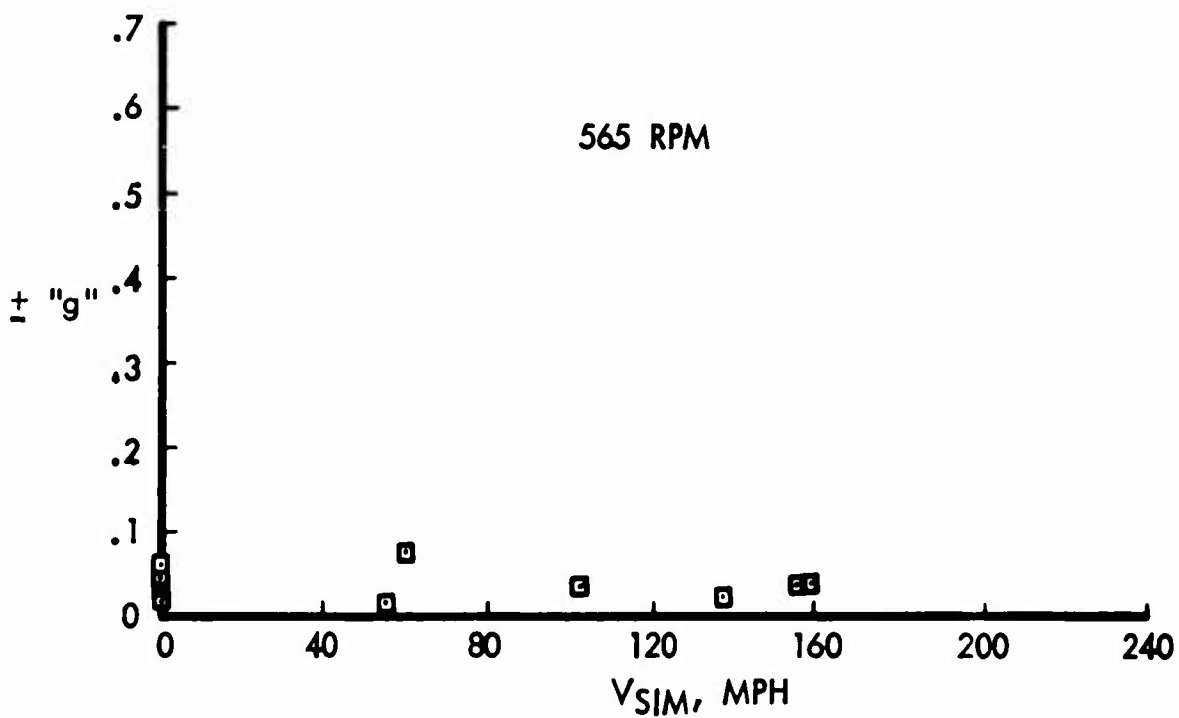


FIG. 48 - LONGITUDINAL BODY VIBRATION VS FWD. SPEED, 6-BLADE ROTOR

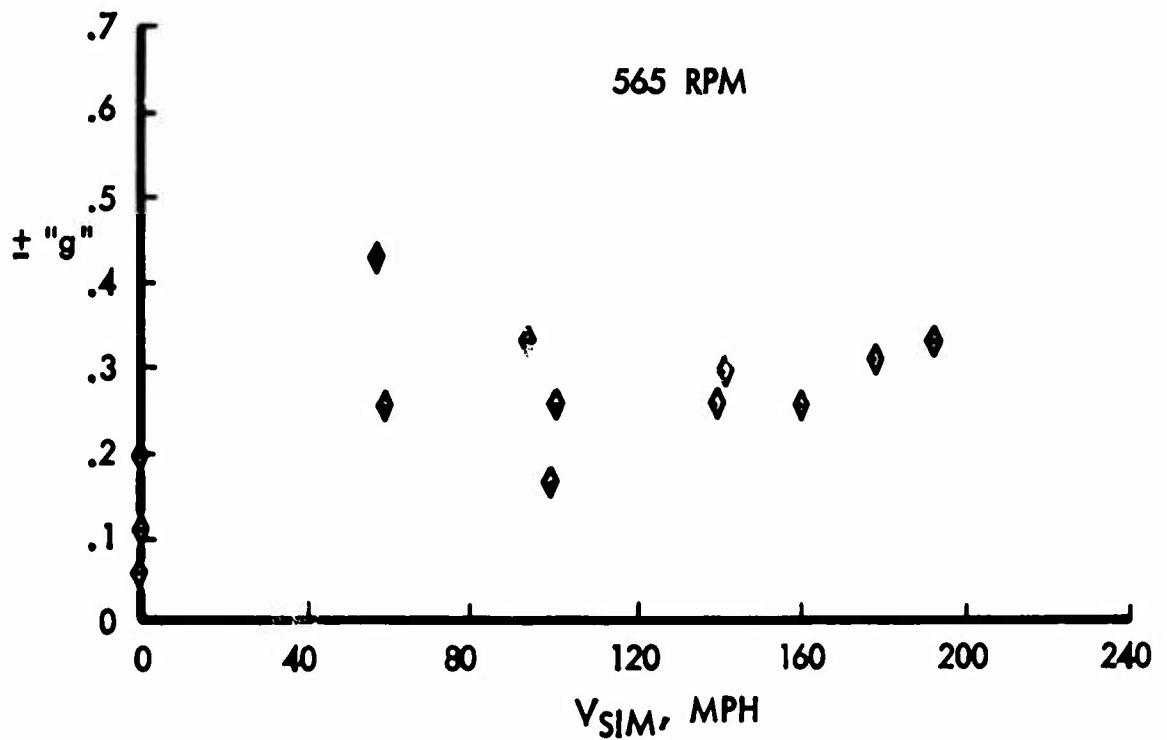


FIG. 49 - LATERAL BODY VIBRATION VS FWD. SPEED, 4-BLADE ( $-6^{\circ}$  TWIST) ROTOR

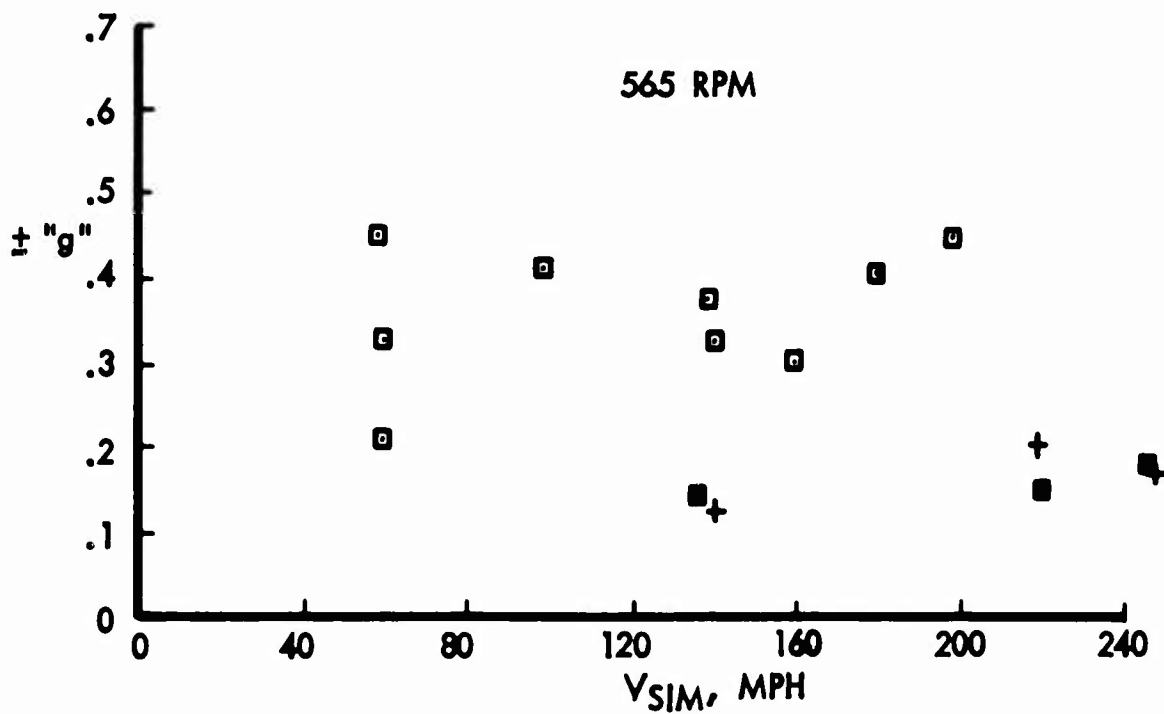


FIG. 50 - LATERAL BODY VIBRATION VS FWD. SPEED, 4-BLADE ROTOR

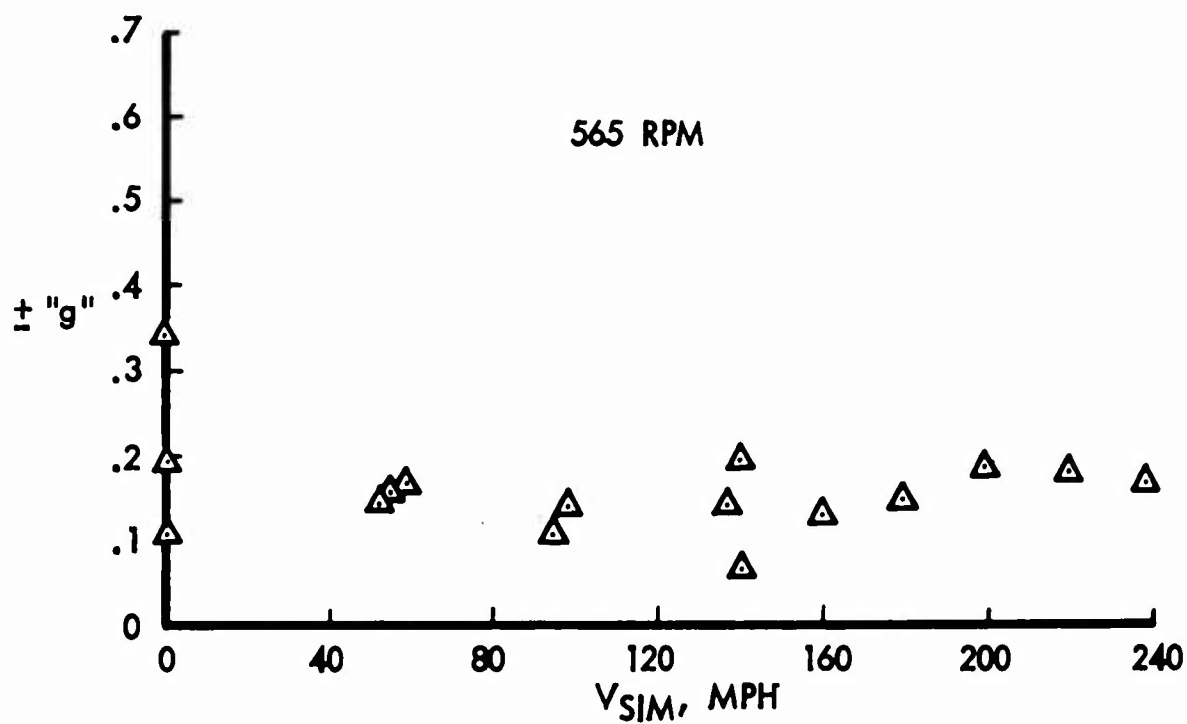


FIG. 51 - LATERAL BODY VIBRATION VS FWD. SPEED, 3-BLADE ROTOR

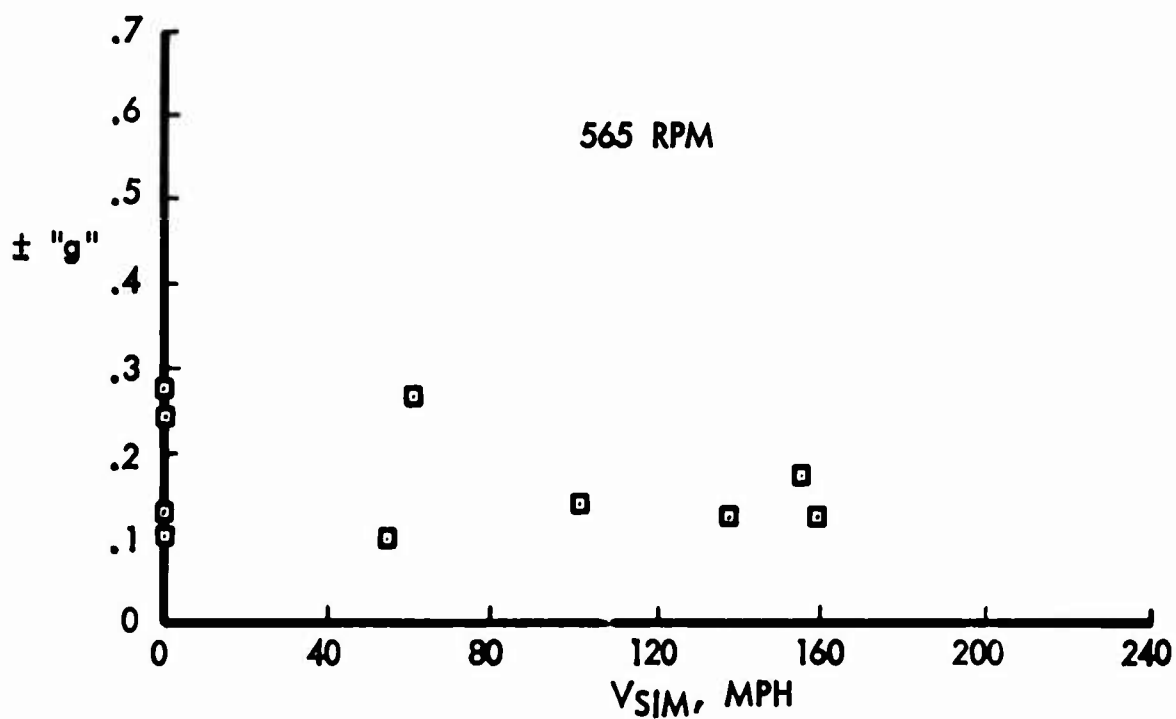


FIG. 52 - LATERAL BODY VIBRATION VS FWD. SPEED, 6-BLADE ROTOR



## DISTRIBUTION

U. S. Army Materiel Command	1
U. S. Army Mobility Command	2
U. S. Army Aviation Materiel Command	2
U. S. Army Transportation Research Command	37
U. S. Army Research and Development Group (Europe)	2
U. S. Army Engineer Research and Development Laboratories	2
Army Research Office-Durham	2
U. S. Army Combat Developments Command	
Armor Agency	1
U. S. Army Transportation School	1
U. S. Army Aviation School	1
U. S. Army Aviation Test Board	1
U. S. Army Aviation Test Activity	2
Air Force Systems Command, Wright-Patterson AFB	2
Air Force Flight Test Center, Edwards AFB	1
Air University Library	1
Bureau of Naval Weapons	3
U. S. Naval Postgraduate School	1
Naval Air Test Center	1
David Taylor Model Basin	1
Ames Research Center, NASA	2
NASA-LRC, Langley Station	6
NASA Representative, Scientific and Technical Information Facility	2
Marine Corps Liaison Officer, U. S. Army Transportation School	1
Research Analysis Corporation	1
National Aviation Facilities Experimental Center	1
U. S. Army Standardization Group, Canada	1
Canadian Liaison Officer U. S. Army Transportation School	1
U. S. Army Standardization Group, U. K.	5
Defense Documentation Center	20

<p>Lockheed-California Company, Burbank, California, Report No. 17790, November 1964, 55 pp. (Contract DA 44-177-AMC-78(T)) USATRECOM Task 1D121401A142</p> <p>Unclassified Report</p>	<p>1. Wind Tunnel Tests of an Optimized Matched Stiffness Rigid Rotor</p>	<p>Lockheed-California Company, Burbank, California, Report No. 17790, November 1964, 55 pp. (Contract DA 44-177-AMC-78(T)) USATRECOM Task 1D121401A142</p> <p>Unclassified Report</p>	<p>1. Wind Tunnel Tests of an Optimized Matched Stiffness Rigid Rotor</p>
<p>2. Contract DA 44-177-AMC-78 (T)</p> <p>An experimental investigation of 10-foot diameter rigid rotors was conducted with the cooperation of the NASA Langley Research Center by the Lockheed-California Company during March 1964. Four configurations differing only in number of blades and blade twist were tested at full scale Reynolds number and Mach number in the Freon atmosphere of the NASA</p>	<p>2. Contract DA 44-177-AMC-78 (T)</p> <p>1. Wind Tunnel Tests of an Optimized Matched Stiffness Rigid Rotor</p>	<p>2. Contract DA 44-177-AMC-78 (T)</p> <p>An experimental investigation of 10-foot diameter rigid rotors was conducted with the cooperation of the NASA Langley Research Center by the Lockheed-California Company during March 1964. Four configurations differing only in number of blades and blade twist were tested at full scale Reynolds number and Mach number in the Freon atmosphere of the NASA</p>	<p>2. Contract DA 44-177-AMC-78 (T)</p> <p>1. Wind Tunnel Tests of an Optimized Matched Stiffness Rigid Rotor</p>
<p>(over)</p> <p>Lockheed-California Company, Burbank, California, Report No. 17790, November 1964, 55 pp. (Contract DA 44-177-AMC-78(T)) USATRECOM Task 1D121401A142</p> <p>Unclassified Report</p>	<p>(over)</p> <p>1. Wind Tunnel Tests of an Optimized Matched Stiffness Rigid Rotor</p>	<p>(over)</p> <p>Lockheed-California Company, Burbank, California, Report No. 17790, November 1964, 55 pp. (Contract DA 44-177-AMC-78(T)) USATRECOM Task 1D121401A142</p> <p>Unclassified Report</p>	<p>(over)</p> <p>1. Wind Tunnel Tests of an Optimized Matched Stiffness Rigid Rotor</p>
<p>2. Contract DA 44-177-AMC-78 (T)</p> <p>An experimental investigation of 10-foot diameter rigid rotor was conducted with the cooperation of the NASA Langley Research Center by the Lockheed-California Company during March 1964. Four configurations differing only in number of blades and blade twist were tested at full scale Reynolds number and Mach number in the Freon atmosphere of the NASA</p>	<p>2. Contract DA 44-177-AMC-78 (T)</p> <p>2. Contract DA 44-177-AMC-78 (T)</p>	<p>2. Contract DA 44-177-AMC-78 (T)</p> <p>An experimental investigation of 10-foot diameter rigid rotor was conducted with the cooperation of the NASA Langley Research Center by the Lockheed-California Company during March 1964. Four configurations differing only in number of blades and blade twist were tested at full scale Reynolds number and Mach number in the Freon atmosphere of the NASA</p>	<p>2. Contract DA 44-177-AMC-78 (T)</p> <p>2. Contract DA 44-177-AMC-78 (T)</p>

#### Langley Transonic Dynamics Tunnel.

All the rotors tested employed a flexure element in place of hub bearings. The in-plane stiffness of the flexure was matched to its flapwise stiffness. Tests to simulated air speeds of 263 miles per hour were successful. This new type of rigid rotor appears to offer advantages by reducing:

- (1) Rotor Weight
- (2) Gyro Weight and Drag
- (3) Hub Drag
- (4) Control Forces
- (5) Mechanical Complexity

#### Langley Transonic Dynamics Tunnel.

All the rotors tested employed a flexure element in place of hub bearings. The in-plane stiffness of the flexure was matched to its flapwise stiffness. Tests to simulated air speeds of 263 miles per hour were successful. This new type of rigid rotor appears to offer advantages by reducing:

- (1) Rotor Weight
- (2) Gyro Weight and Drag
- (3) Hub Drag
- (4) Control Forces
- (5) Mechanical Complexity

#### Langley Transonic Dynamics Tunnel.

All the rotors tested employed a flexure element in place of hub bearings. The in-plane stiffness of the flexure was matched to its flapwise stiffness. Tests to simulated air speeds of 263 miles per hour were successful. This new type of rigid rotor appears to offer advantages by reducing:

- (1) Rotor Weight
- (2) Gyro Weight and Drag
- (3) Hub Drag
- (4) Control Forces
- (5) Mechanical Complexity

#### Langley Transonic Dynamics Tunnel.

All the rotors tested employed a flexure element in place of hub bearings. The in-plane stiffness of the flexure was matched to its flapwise stiffness. Tests to simulated air speeds of 263 miles per hour were successful. This new type of rigid rotor appears to offer advantages by reducing:

- (1) Rotor Weight
- (2) Gyro Weight and Drag
- (3) Hub Drag
- (4) Control Forces
- (5) Mechanical Complexity